Journal of Geochemical Exploration 130 (2013) 22–43

Contents lists available at SciVerse ScienceDirect

Journal of Geochemical Exploration

journal homepage: www.elsevier.com/locate/jgeoexp

Oxidation state of iron in alteration minerals associated with sandstone-hosted unconformity-related uranium deposits and apparently barren alteration systems in the Athabasca Basin, Canada: Implications for exploration

Ronald Ng [a,*], Paul Alexandre [a], Kurt Kyser [a], Jonathan Cloutier [b], Yassir A. Abdu [c], Frank C. Hawthorne [c]

[a] Department of Geologic Sciences and Geological Engineering, Queen's University, Kingston, Ontario K7L 3N6, Canada
[b] CSIRO Earth Science & Resource Engineering, 26 Dick Perry Ave., Kensington, Western Australia, Australia
[c] Department of Geological Sciences, University of Manitoba, Winnipeg, Manitoba R3T 2N2, Canada

ARTICLE INFO

Article history:
Received 26 September 2012
Accepted 28 February 2013
Available online 20 March 2013

Keywords:
Athabasca Basin
Sandstone-hosted unconformity-related uranium
Iron oxidation state
Illite
Chlorite

ABSTRACT

Sandstone-hosted unconformity-related U deposits in the Athabasca Basin at McArthur River Zone 4 and Maurice Bay as well as barren alteration systems at Wheeler River Zone "K" and Spring Point are surrounded by an outer, peripheral zone of illite and an inner, central zone of chlorite alteration. The oxidation state of Fe determined by ^{57}Fe Mössbauer spectroscopy of illite, sudoite, and clinochlore from these systems indicates that pre-ore illite contains mostly Fe^{3+} ($Fe^{3+}/\Sigma Fe = 0.77–1.00$), reflecting formation from a predominantly oxidizing basinal fluid. Lower $Fe^{3+}/\Sigma Fe$ ratios are recorded by late pre-ore sudoite and clinochlore occurring near faulted unconformities, consistent with the contribution to the chlorites from reducing basement-derived fluids. Sudoite and clinochlore in the alteration halo of barren systems are more reduced ($Fe^{3+}/\Sigma Fe$ median = 0.3–0.4) than sudoite from mineralized systems ($Fe^{3+}/\Sigma Fe$ median = 0.45–0.55). Sudoite from both systems becomes broadly more oxidized with increasing distance from the fault zone. Variations in the $Fe^{3+}/\Sigma Fe$ ratios of sudoite and clinochlore support a mechanism in which Fe^{2+} transported by reducing basement-derived fluids is partially oxidized to Fe^{3+} by basinal fluids prior to incorporation into the chlorite. Thus, scarcity of oxidizing U-bearing basinal fluids available for interaction with reducing basement fluids is a critical factor precluding U mineralization in barren systems. Trends of decreasing $Fe^{3+}/\Sigma Fe$ ratios in sudoite coupled with decreasing $^{207}Pb/^{206}Pb$ ratios of leachable Pb can be used as geochemical vectors to the sites of potential U mineralization.

1. Introduction

The Paleo–Mesoproterozoic Athabasca Basin, located in northern Saskatchewan and Alberta, Canada, hosts high-grade, large-tonnage unconformity-related U deposits (Fig. 1). These deposits are situated near faults and shear zones that intersect the unconformity between Athabasca Group sedimentary rocks and Archean to Paleoproterozoic metamorphic basement rocks (Kyser and Cuney, 2008). U deposition occurs at a stationary redox front (Quirt, 1986), where oxidizing uraniferous basinal brines encounter reducing basement lithologies (Alexandre et al., 2005; Hoeve and Sibbald, 1978; Komninou and Sverjensky, 1996) or reducing basement-derived fluids (Fayek and Kyser, 1997; Kotzer and Kyser, 1995; Wilson and Kyser, 1987). Alternatively, it has been proposed that the reducing fluids did not originate from a distinct basement source but were basinal fluids that became chemically-modified via interaction with basement rocks (Derome et al., 2005; Mercadier et al., 2012; Richard et al., 2010).

In sandstone-hosted systems, which are the focus of this study, significant clay alteration is found surrounding the main ore-controlling structures (e.g. Cigar Lake, McArthur River). Alteration can extend up to 400 m wide along the base of the Athabasca Group, several thousand meters along strike, and reach several hundred meters above the unconformity (Jefferson et al., 2007). These halos are typically characterized by a narrow central zone of chlorite alteration (di-trioctahedral and trioctahedral) and a spatially-extensive peripheral zone of illite/muscovite alteration. However, similar alteration patterns can be present in the absence of mineralization (Alexandre et al., 2009a; Cloutier et al., 2010). These apparently barren alteration systems are interpreted as forming when stationary redox fronts fail to establish, thus preventing the focused precipitation and accumulation of U (Quirt, 1986) or when U-bearing oxidizing fluids are unavailable for interaction with reducing basement-derived fluids (Alexandre et al., 2009a; Cloutier et al., 2010).

The crystal structure and chemistry of clay minerals can provide a record of the physico-chemical conditions during alteration, including temperature (Cathelineau, 1988; Zang and Fyfe, 1995), type of fluid (Kotzer and Kyser, 1995; Wilson and Kyser, 1987), geological

* Corresponding author. Tel.: +1 613 5332183; fax: +1 613 5336592.
E-mail address: ng@geoladm.geol.queensu.ca (R. Ng).

0375-6742/$ – see front matter © 2013 Elsevier B.V. All rights reserved.
http://dx.doi.org/10.1016/j.gexplo.2013.02.009

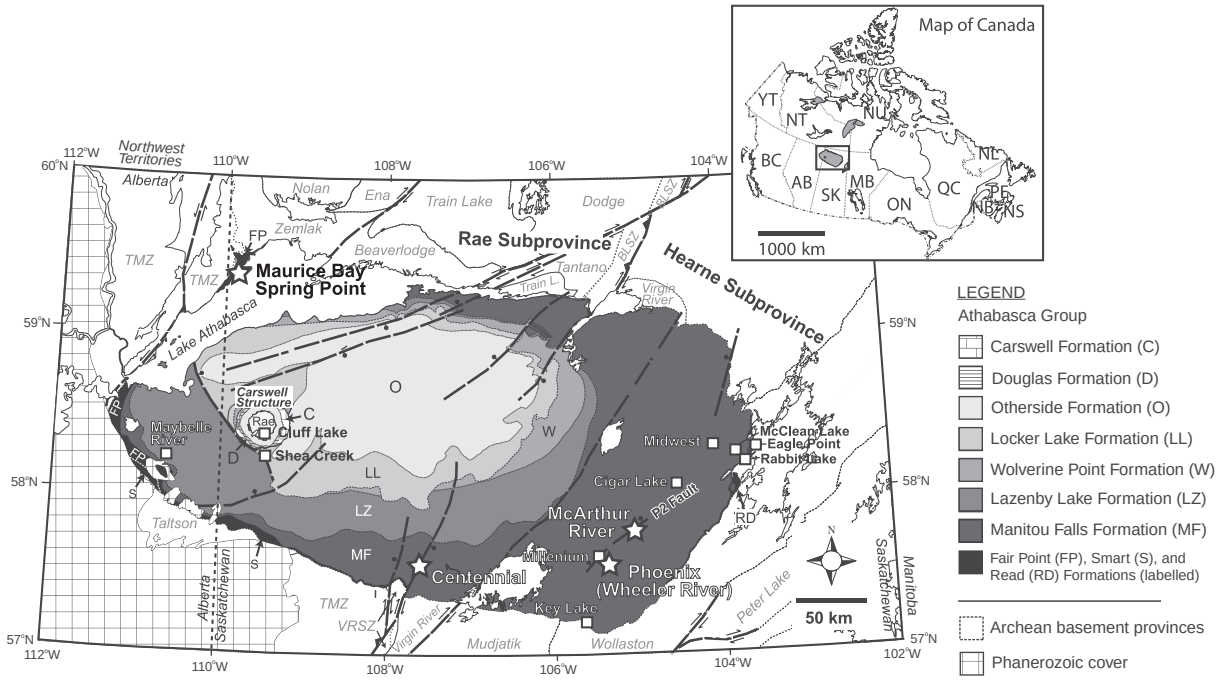

Fig. 1. Generalized geologic map of the Athabasca Basin in Northern Saskatchewan, Canada. Major basement structural subprovinces (bold), domains (italic), fault structures (dashed lines), stratigraphic divisions, and unconformity-related U deposits, including those from this study (stars), are indicated (modified after Hoffman, 1989; Ramaekers et al., 2007). Abbreviations: BLSZ = Black Lake Shear Zone, TMZ = Taltson Magmatic Zone, VRSZ = Virgin River Shear Zone.

setting (Hinckley, 1963; Zhang et al., 2001), timing of formation and subsequent alteration events (Alexandre et al., 2009b). However, the redox condition during alteration, a parameter which can be inferred from the oxidation state of Fe in alteration minerals, has received only limited attention (Billault et al., 2002).

Fe^{2+} is a potential reductant for U^{6+} in unconformity-related U deposits, based on the close spatial and temporal association between hematite and U ore bodies (e.g. Alexandre et al., 2005; Wallis et al., 1985). In illite, di-trioctahedral chlorite (e.g. sudoite), and trioctahedral chlorite (e.g. clinochlore), Fe^{2+} and Fe^{3+} can substitute at the octahedrally coordinated sites and Fe^{3+} into the tetrahedrally coordinated sites (Billault et al., 2002; Percival and Kodama, 1989; Weaver et al., 1967). Substitution of Fe^{3+} into the tetrahedral site is considered rare in chlorite (Zazzi et al., 2006) and mainly restricted to illite with >5 wt.% total Fe (Murad and Wagner, 1994).

In this study, ^{57}Fe Mössbauer spectroscopy is used to quantify the oxidation state of Fe in paragenetically-constrained illite and both di-trioctahedral and trioctahedral chlorites from several sandstone-hosted alteration systems in the Athabasca Basin. These include alteration systems that are mineralized (McArthur River Zone 4, Maurice Bay), apparently barren (Wheeler River Zone "K", Spring Point), and proximal to mineralization at the Centennial deposit. The premise for this study is that fluid composition influences the observed mineral paragenesis and crystal chemistry (Kister et al., 2005; Komninou and Sverjensky, 1996), and therefore, the redox environment in which the fluid existed should be reflected in the valence state of structural Fe in the alteration mineral (Fanning et al., 1989). The objectives of this study include: (1) mapping the temporal and spatial evolution of the redox environment around these five sandstone-hosted alteration systems; (2) elucidating the mechanism controlling the oxidation state of Fe in clay alteration and the critical geochemical requirement for U mineralization; (3) evaluating potential post-crystallization changes to the Fe oxidation state in phyllosilicates; and (4) assessing the application of Fe oxidation state in clay alteration to U exploration by comparing it to known geochemical vectors for U mineralization.

2. Geological considerations

2.1. Regional-scale geology

The late Paleo- to Mesoproterozoic Athabasca Basin, located in northern Saskatchewan and Alberta, Canada, overlies the Rae and Hearne subprovinces of the Western Churchill Province (Fig. 1). These Archean cratons comprise granitoids and volcano-sedimentary supracrustal rocks overlain by Paleoproterozoic metasedimentary and metavolcanic rocks (Berman et al., 2007; Hanmer et al., 2004; Hoffman, 1988; Lewry and Sibbald, 1980). The Rae and Hearne cratons are bounded to the west by the ca. 2.0 to 1.9 Ga Taltson–Thelon Magmatic Zone (Berman and Bostock, 1997), to the southeast by the ca. 1.86 to 1.76 Ga Trans-Hudson Orogen (Annesley et al., 2005), and are welded by the ca. 1.9 Ga Snowbird Tectonic Zone (Berman et al., 2007; Hoffman, 1988).

The Athabasca Basin formed between ca. 1760 Ma and ca. 1500 Ma in response to rapid exhumation of the Trans-Hudson Orogen (Ramaekers et al., 2007). Fluvial sediments filled three NE–SW-oriented sub-basins (Jackfish, Mirror, and Cree) that coalesced into the Athabasca Basin (Ramaekers, 1990; Ramaekers et al., 2001). The basin fill consists mostly of quartzose sandstone with minor siltstone, conglomerate, mudstone, and dolostone, comprising the Athabasca Group (Fig. 1). The Athabasca Group is subdivided into four flat-lying, upward-fining, unconformity-bounded sequences (Ramaekers et al., 2007). These include, in ascending order, the basal Fair Point Formation; the Read, Smart, Manitou Falls, and Reilly Lake Formations, the Lazenby Lake and Wolverine Point Formations; and the Locker Lake, Otherside, Douglas, and Carswell Formations (Fig. 1). At McArthur River and Wheeler River, which are located east of the Virgin River Shear Zone, the Read Formation replaces the informal MFa member of Ramaekers (1990) and the Manitou Falls Formation is subdivided into the Bird (MFb), Collins (MFc), and Dunlop (MFd) members. Fluid inclusion homogenization temperatures recorded in quartz overgrowths (Pagel et al., 1980) suggest that the total thickness of the Athabasca Group may have reached 5–7 km during the Mesoproterozoic. Northwest-striking dikes (Cumming and

Krstic, 1992), emplaced during the 1267 ± 2 Ma Mackenzie thermal event (LeCheminant and Heaman, 1989), intrude into the Athabasca Basin and underlying metamorphic basement.

U–Pb dating of uraninite and $^{40}Ar/^{39}Ar$ dating of syn-ore illite from several sandstone- and basement-hosted deposits indicate that the main stage of U mineralization in the Athabasca Basin occurred at ca. 1590 Ma (Alexandre et al., 2009b). Far-field tectonic activity induced multiple episodes of basin-wide fluid circulation following initial U mineralization causing resetting of the U–Pb isotope system of uraninite and the alteration of U-bearing minerals (Alexandre et al., 2009b; Fayek et al., 2002).

2.2. Deposit-scale geology

2.2.1. McArthur River Zone 4

The McArthur River deposit is located near the southeastern margin of the Athabasca Basin and overlies the Wollaston Domain of the Hearne craton (Fig. 1). The deposit has average ore grades of 20.69% U_3O_8 (17.55% U) and combined proven and probable reserves of 332.6 Mlbs U_3O_8 (Bronkhorst et al., 2009). McArthur River comprises five sandstone-hosted ore bodies (Zones 1, 3, 4, A, B) and one basement-hosted ore body (Zone 2) (Fig. 2A). The McArthur River ore bodies are structurally-controlled by the NE-striking, SE-dipping, P2 reverse fault (McGill et al., 1993). Samples from this study were obtained from the sandstone-hosted Zone 4 alteration system (Fig. 2B). The Zone 4 ore body occurs at depths of 500–570 m and is hosted partially within the graphite-bearing pelitic gneiss hanging wall of the Wollaston Group and sandstones and fanglomerates of the basal Read Formation (McGill et al., 1993). Alteration within the Read and Manitou Falls Formations includes silicification, desilicification, hematite, dickite, dravite, illite, sudoite, and kaolinite with illite, sudoite, and clinochlore present in the basement rocks near the deposit (Alexandre et al., 2005; Derome et al., 2005; Kotzer and Kyser, 1995). Early pre-compaction quartz cementation (Hiatt et al., 2007) caused extensive silicification of the Read Formation and lower MFb at McArthur River that limited the spatial extent of sudoite alteration around the deposit (McGill et al., 1993; Mwenifumbo et al., 2004).

2.2.2. Wheeler River Zone "K"

The apparently barren Zone "K" alteration system in the Wheeler River property is located approximately 35 km southwest of McArthur River (Figs. 1, 2C). The Wheeler River property also contains the high-grade sandstone-hosted Phoenix mineralization (Arseneau and Revering, 2010; Kerr, 2010), although only weak mineralization in the basement (0.17% U_3O_8 over 7.7 m) was intersected at Zone K (Gamelin et al., 2010). The Athabasca Group at Zone "K" is represented by the Read and Manitou Falls Formations (MFb, MFc, MFd). The underlying basement rocks comprise graphitic and non-graphitic pelitic gneisses, meta-arkoses, psammites, metaquartzite, and calc-silicate gneisses of the Wollaston Group with graphitic shear zones forming part of a reverse fault system at the center of Zone "K" (Cloutier et al., 2010). The alteration assemblage within the Athabasca Group sandstones includes quartz, Fe oxides, dickite, muscovite, dravite, sudoite, and kaolinite. The Zone "K" alteration system is characterized by a

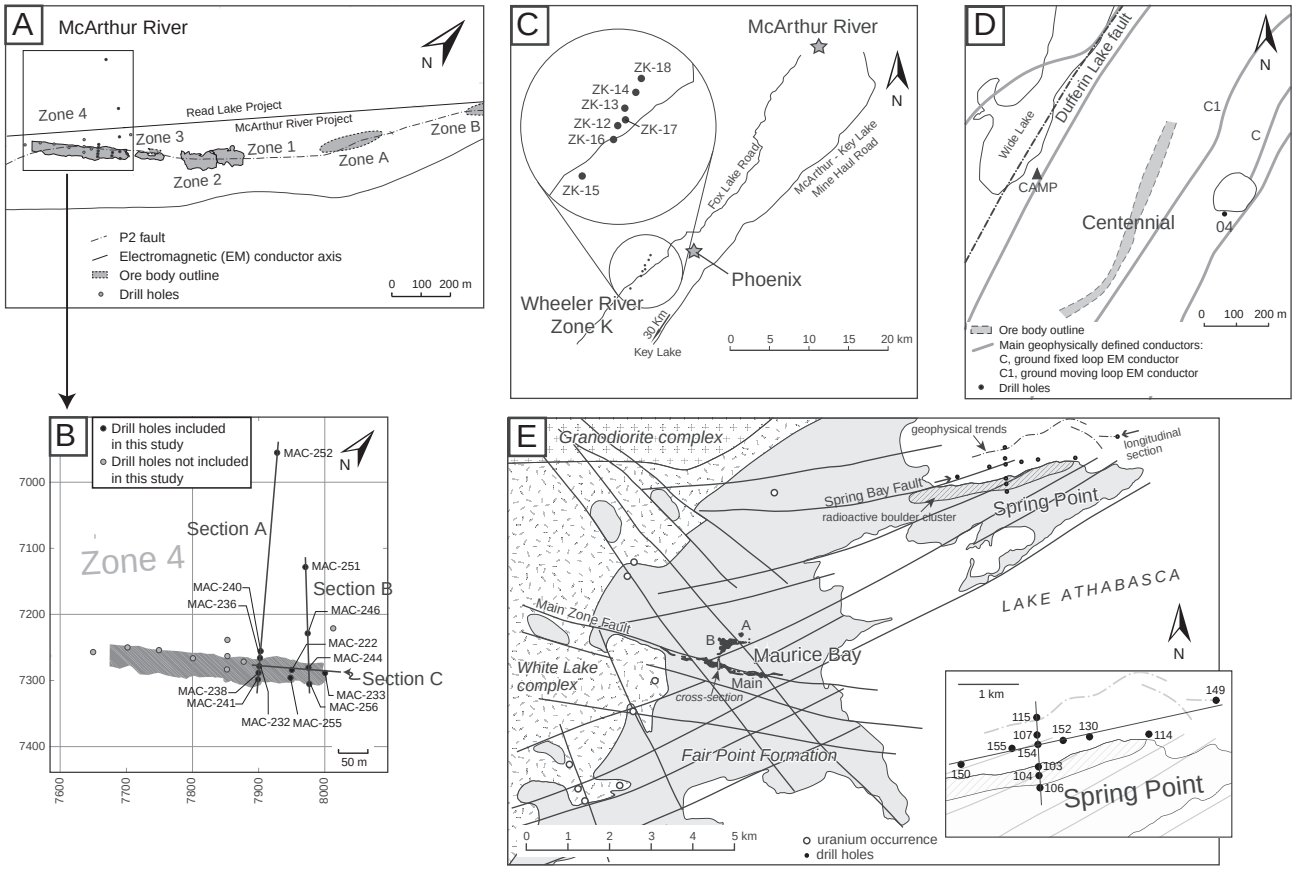

Fig. 2. A. Plan view of the McArthur River property. The major sandstone-hosted (Zone 1, 3, 4, A, B) and basement-hosted (Zone 2) ore bodies coincide with an electromagnetic conductor corresponding to the graphite-bearing P2 reverse fault. B. McArthur River Zone 4 ore body in plan view. Drill holes in this study are from the eastern half of Zone 4 and delineate two NW–SE-oriented transects (Line A and B) and one SW–NE-oriented transect (Line C). C. Plan view of the Wheeler River area. Drill holes in this study delineate a SSW–NNE-oriented transect through the Zone "K" trend (modified after Cloutier et al., 2010). D. Plan view of the Centennial deposit. Major electromagnetic conductors determined by airborne geophysics are indicated (modified after Alexandre et al., 2012). Location of drill-hole VR-04 (this study) is indicated. E. Simplified geologic map of the southern and central parts of the Maurice Bay area (modified after Harper, 1996). Position of Maurice Bay ore bodies (A, B, Main) and drill holes are indicated. Inset: Enlarged map of the Spring Point area. Drill holes sampled at Spring Point delineate a WSW–ENE-oriented and SSE–NNW-oriented transect.

250 m-high by 500 m-wide clinochlore alteration halo in the sandstones overlying the basement shear zone (Cloutier et al., 2010).

2.2.3. Centennial, Virgin River

The Centennial deposit, located in the south-central Athabasca Basin, overlies the Virgin River domain of the Hearne craton (Figs. 1, 2D). The Athabasca Group at Centennial includes the Read Formation overlain by MFc and MFd, with MFb being absent. This sandstone-hosted deposit occurs at a depth of 800 m and is hosted in the basal sandstones of the Read Formation and up to 30 m into the basement rocks (Alexandre et al., 2012; Jiricka and Witt, 2008). Drill hole VR-04, located approximately 240 m east-northeast of the Centennial ore body, intersected weak mineralization near the unconformity, with one sample (VR04-821) containing about 0.05% U_3O_8 (Fig. 2D; Alexandre, pers. comm.). The underlying basement belongs to the Virgin River Schist Group and consists of granitoid in the footwall and metasedimentary and metavolcanic rocks in the hanging wall (Reid et al., 2011). The Centennial deposit differs from typical sandstone-hosted unconformity-related U deposits as it is not hosted by a major basement fault structure rooted in graphitic basement units (Alexandre et al., 2012; Reid et al., 2010). The NE–SW-oriented Dufferin Lake thrust fault—the major fault structure in the area—is located ca. 300–400 m northwest of the Centennial deposit (Fig. 2D). The main sandstone alteration includes silicification, desilicification, kaolinite, dravite, illite, sudoite, and hematite (Alexandre et al., 2012). Basement alteration consists of a distal trioctahedral chlorite (chamosite and Fe–Mg clinochlore) and proximal illite–sudoite alteration (Reid et al., 2011). Diabase dikes and sills, emplaced during the Mackenzie dike event, intrude into the Centennial ore body (Alexandre et al., 2012; Reid et al., 2010).

2.2.4. Maurice Bay

The sandstone-hosted Maurice Bay sub-economic deposit is located near the northwestern margin of the Athabasca Basin and overlies the Zemlak domain of the Rae subprovince (Figs. 1, 2E). The deposit contains a historical resource of about 1.5 Mlbs U_3O_8 at an average ore grade of 0.6% U_3O_8 (Mega Uranium Ltd., 2012). U mineralization at Maurice Bay occurs in three zones (A, B, and Main), at depths of 50–75 m, and is hosted in the basal Fair Point Formation and underlying pelitic and migmatitic gneisses of the White Lake basement complex (Card, 2001; Harper, 1996). The Maurice Bay deposit is structurally-controlled by syn- and post-Athabasca reactivated basement faults, which are oriented east-northeast, east-southeast, and northwest, and form part of a series of horst-and-graben structures (Fig. 2E). The alteration assemblage in the sandstone consists of quartz, hematite, kaolinite, illite, and sudoite, with strong hematite alteration associated with U mineralization (Alexandre et al., 2009a).

2.2.5. Spring Point

The apparently barren Spring Point alteration system is located approximately 8.5 km northeast of Maurice Bay and both are situated within similar geological settings (Fig. 1). The Spring Point alteration system lies on the minimally-displaced Spring Bay Fault, which is part of the fracture pattern controlling the topography of the Maurice Bay area (Fig. 2E). Pervasive hydrothermal alteration of the Fair Point Formation sandstones above the Spring Bay fault forms a bell-shaped anomalous zone about 2600 m in length and up to 400 m wide at the unconformity (Quirt, 1986). The alteration assemblage in the Fair Point Formation is similar to the Maurice Bay deposit and is characterized by kaolinite overprinted by illite and sudoite (Quirt, 1986) but differs by a lower intensity of alteration (Alexandre et al., 2009a). The Spring Point alteration zone is characterized by a reduced central core, indicated by hematite dissolution and disseminated pyrite and chalcopyrite (Quirt, 1986). Although anomalous U was detected near the faulted unconformity, U concentrations are uniformly low within the alteration zone and similar to background values in the Athabasca Group sandstones (ca. 1.5 ppm; Alexandre et al., 2009a; Quirt, 1985).

3. Methodology

3.1. Sample preparation and analyses

Drill core samples were collected from the alteration systems at McArthur River Zone 4, Wheeler River Zone "K", Centennial, Maurice Bay, and Spring Point. At the McArthur River deposit, 13 diamond drill holes, both mineralized and non-mineralized, from the eastern half of the Zone 4 ore body were sampled (Fig. 2B). These drill holes delineate two subparallel northwest–southeast-oriented transects (section A, section B) and one southwest–northeast-oriented transect (section C). Samples were selected from various alteration horizons within the Read and Manitou Falls Formations overlying the Zone 4 mineralization with a focus on selecting drill cores containing the greatest abundance of illite or di-trioctahedral chlorite. These include samples from the di-trioctahedral chlorite-rich (labeled C1) zone along the MFc–MFd boundary (9), mixed illite and illite–chlorite mixed layer clay zone (3), monomineralic illite zone (13), mixed illite–dickite zone (2), and mixed illite–kaolinite samples (2) from the basal fanglomerate (Fig. 5). Seven samples were also chosen from the di-trioctahedral chlorite-rich (labeled C2) alteration halo in the basal Read Formation surrounding the mineralization. On the Wheeler River property, samples were chosen from seven exploration drill holes, delineating a south-southwest to north-northeast transect through the apparently barren Zone "K" alteration system (Fig. 2C). Samples were selected from the zones of illite (8), di-trioctahedral chlorite (4), and trioctahedral chlorite (4) alteration within the Read and Manitou Falls Formations around the Zone "K" shear zone (Fig. 6). Near the Centennial deposit, five di-trioctahedral chlorite samples occurring at ca. 600–820 m depth were chosen from the Read Formation and Manitou Falls c and d members intersected by drill hole VR-04 (Figs. 2D, 7). At the Maurice Bay deposit, di-trioctahedral chlorite samples (4) were selected from two mineralized (MB41, MB146) and one non-mineralized (MB726) drill hole that form part of a north–south transect through the Main ore body (Figs. 2E, 8). At the apparently barren Spring Point alteration system, di-trioctahedral chlorite samples were selected from five drill holes from two transects: a WSW–ENE-oriented transect and a SSE–NNW-oriented transect (Fig. 2E). Three samples occurred near the upper portions of drill holes and four occurred near the unconformity at the center of the system (Fig. 9).

Alteration minerals were extracted from crushed drill cores by ultrasonic disintegration and centrifuged into the 2–5 μm and <2 μm fractions. These separates were analyzed by X-ray diffraction (XRD) to determine their mineralogy and modal abundance. Whole-rock chemical analysis of the mineral separates was not performed in this study for estimating modal abundances because it would be difficult to distinguish the various alteration minerals since they contain similar elements, exhibit cation substitution, and form interlayered clays.

For each system, a mineral paragenesis was formulated from the petrographic observation of polished thin sections using transmitted and reflected light microscopy. These have been combined into a generic paragenesis, albeit with several differences among them (Fig. 3). The chemical compositions of the alteration minerals were determined by electron probe microanalysis (EPMA). In this study, the term 'illite' is used to refer to Athabasca Basin white mica which has an intermediate chemical composition between illite and muscovite. Formation temperatures were calculated for illite using the molar fractionation of pyrophyllite (Cathelineau, 1988) and for chlorite using $^{[4]}$Al site occupancy (Cathelineau, 1988; Walshe, 1986; Zang and Fyfe, 1995). The uncertainty in the calculated temperatures based on these empirical geothermometers is ±25 °C.

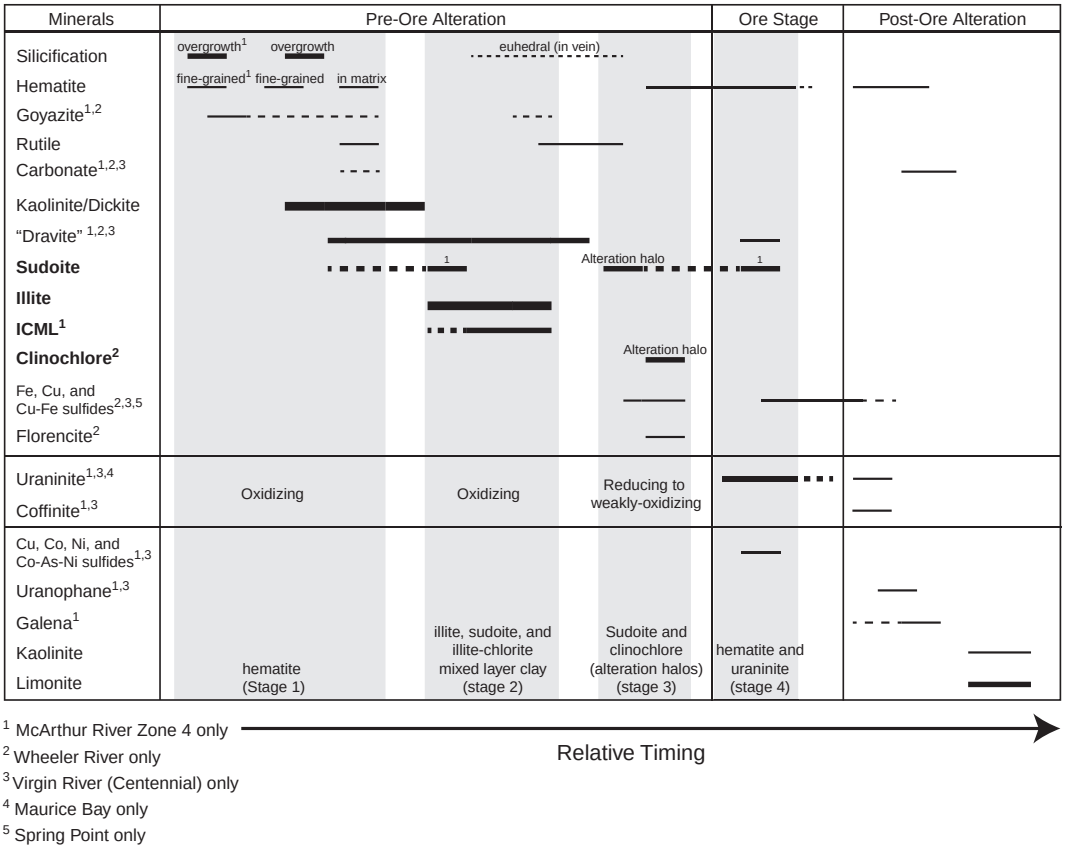

Fig. 3. Generalized mineral paragenesis in Athabasca Group and ore zone for sandstone-hosted alteration systems, combining paragenesis from McArthur River Zone 4, Wheeler River, Virgin River project and Centennial deposit, Maurice Bay, and Spring Point. Minerals measured by Mössbauer spectroscopy are indicated in bold.

The hydrogen and oxygen isotopic compositions of alteration minerals were used to characterize the fluids from which they formed. Oxygen isotopic compositions were determined by the BrF_5 extraction method of Clayton and Mayeda (1963) and measured using a dual-inlet MAT252 isotope ratio mass spectrometer (IRMS). Hydrogen isotopic compositions were analyzed using a ThermoFinnigan thermal conversion elemental analyzer (TC/EA) linked to a Delta^{Plus}XP IRMS. Results for oxygen and hydrogen isotope ratios are expressed using conventional delta (δ) notation in units of per mil (‰) relative to Vienna Standard Mean Ocean Water (V-SMOW). The oxygen isotope fractionation factors of Eslinger and Savin (1973) were used for illite-water and Wenner and Taylor (1971) for chlorite-water. For hydrogen isotopes, the fractionation factors of Yeh (1980) were used for illite-water and Marumo et al. (1980) for chlorite-water.

The isotopic composition of leachable Pb from crushed drill cores (>1.14 mm fraction) was determined using a 2% HNO_3 leach technique and measured by high-resolution inductively-coupled plasma mass spectrometry (HR-ICP-MS), following the method of Holk et al. (2003). The $^{207}Pb/^{206}Pb$ ratios of leachable Pb from drill core have been demonstrated as a vector for unconformity-related U deposits in the Athabasca Basin (Alexandre et al., 2012; Cloutier et al., 2009; Holk et al., 2003). Low Pb isotope ratios ($^{207}Pb/^{206}Pb < 0.7$) may indicate proximity to a source of high U concentration, such as a Proterozoic U ore body, or the mobilization of radiogenic components from a deposit during post-ore fluid events which may affect the Fe system in the clay minerals.

3.2. Mössbauer spectroscopy

The structural and valence state of Fe in phyllosilicates was determined by ^{57}Fe Mössbauer spectroscopy at the University of Manitoba (Canada). Samples were mineral separates extracted from drill cores from different parts of the alteration systems. For select separates, matching whole-rock powders (12 samples) were also measured to compare with results from clay separates. Spectra were acquired at room temperature (RT) using a ^{57}Co (Rh) point source, transmission geometry, and velocity range of ±11 mm/s. Mössbauer absorbers were prepared by grinding approximately 125 mg of powdered sample with sugar under acetone and loading the mixture into a Perspex sample holder (1 cm in diameter). Spectra were processed using the RECOIL software and generally deconvoluted using Voigt-based fitting (Rancourt and Ping, 1991) to a model having one Fe^{2+} site and two Fe^{3+} sites: one quadrupole-splitting distribution (QSD) site and one hyperfine-field-distribution (HFD) site. The Fe^{2+} and Fe^{3+} (QSD) sites yielded doublets which were assigned to Fe in octahedral coordination within phyllosilicates. For the majority of spectra, the Fe^{3+} (HFD) site produced a magnetically split sextet having an isomer shift (0.37 mm/s relative to α-Fe at RT), quadrupole-splitting (0.12 mm/s), and a magnetic field (51 T) characteristic of Fe^{3+} in bulk hematite. In some spectra, particularly those of the Fe-poor illite samples, the Fe^{3+} (HFD) site showed a collapsing sextet(s) with a magnetic field that is much smaller than 51 T, but with an isomer shift and quadrupole-splitting similar to that of hematite, which may be attributed to small-particle hematite. In these spectra, the smaller particles of hematite may give rise to a superparamagnetic contribution that would overlap with the Fe^{3+} (QSD) doublet. To account for this, another HFD-site with a zero magnetic field and a wide HFD was added. The relative area of each Fe site is reported as a percentage (%). The relative abundance of Fe^{2+} and Fe^{3+} contained in phyllosilicates is expressed as the parameter $Fe^{3+}/\Sigma Fe$, where ΣFe equals the sum of Fe^{2+} and Fe^{3+}. Using the Mössbauer and electron microprobe data, mineral formulae for illite and both di-trioctahedral and

trioctahedal chlorites were calculated from oxide weight percentages using anion normalization and partitioning of total Fe (FeO_T) as FeO wt.% and Fe_2O_3 wt.%. As monomineralic separates of di-trioctahedral chlorite could not be obtained at McArthur River Zone 4, the $Fe^{3+}/\Sigma Fe$ ratios for end-member di-trioctahedral chlorite were extrapolated from clay mixtures.

4. Results

4.1. Mineral paragenesis of sandstone-hosted alteration systems

A generalized mineral paragenesis for the studied sandstone-hosted alteration systems is constructed from combining the paragenesis for each system (Fig. 3). Four major Fe-bearing alteration stages are identified including early, mid, and late pre-ore alteration and ore stages. Each stage is characterized by a major Fe-bearing mineral that provides a temporal record of the redox conditions in the alteration fluid.

Stage 1 formed fine-grained hematite as coatings on detrital quartz, inclusions within quartz overgrowths, and coarse-grained hematite crystals (specularite) within interstitial pore spaces during early pre-ore alteration. Stage 2 formed phyllosilicate-dominated alteration assemblages during the mid pre-ore stage and is characterized by early di-trioctahedral chlorite (C1) alteration at McArthur River Zone 4 followed by illite alteration in all five systems. At McArthur River Zone 4, illite alteration of C1 chlorite resulted in an illite–chlorite mixed layer (ICML) clay mineral. This second alteration stage follows diagenetic kaolinite and dickite paragenetically and is coeval with dravite alteration. Stage 3 is characterized by hydrothermal chlorite alteration near faulted unconformities, which in mineralized systems, corresponds to the late pre-ore alteration stage. Hydrothermal chlorite alteration follows illite paragenetically and formed di-trioctahedral chlorite halos at McArthur River Zone 4 (C2 chlorite), Wheeler River Zone "K", Spring Point, Maurice Bay, and Centennial. At the Wheeler River Zone "K" system, hydrothermal di-trioctahedral chlorite alteration is overprinted by a later-forming trioctahedral chlorite halo (Cloutier et al., 2010). In the mineralized systems, it remains possible that late pre-ore di-trioctahedral chlorite alteration may have formed nearly synchronous with U mineralization since evidence for it predating mineralization is based primarily on the petrographic observation of uraninite precipitating in the secondary porosity of clay matrices (Alexandre et al., 2012). As such, there is uncertainty in the paragenetic timing between these two minerals since clear cross-cutting relationships are not well-developed due to di-trioctahedral chlorite grains being flexible and able to reorient when impinged by uraninite. Stage 4 produced hematite alteration coeval with U mineralization. This alteration stage is observed in the ore zones of mineralized alteration systems (e.g. McArthur River Zone 4, Maurice Bay, Centennial) and is characterized by intense hematite overprinting clay matrices.

4.2. Mineral chemistry of alteration minerals

Representative chemical compositions, calculated mineral formulae, and formation temperatures of pre-ore illite, di-trioctahedral chlorite, and trioctahedral chlorite are tabulated for the five sandstone-hosted alteration systems (Table 1) and compared in Fig. 4.

Illite samples from the five studied sandstone-hosted alteration systems have similar chemical compositions and are characterized by K_2O contents between 7.5 and 9.5 wt.% and MgO contents between 0.5 and 1.7 wt.% (Table 1). The Fe contents of illite from the Maurice Bay, Centennial, and McArthur River Zone 4 deposits range between 0.5 and 0.8 wt.% FeO_T, whereas, illite samples from the apparently barren Wheeler River Zone "K" and Spring Point alteration systems have higher Fe contents from 1.2 to 1.7 wt.% FeO_T. Illite from the five alteration systems has K interlayer site occupancy site ranging from 0.67 to 0.83 atoms per formula unit (apfu), $^{[4]}Si/^{[4]}Al$ ratios greater than 3, and less than 0.2 apfu substitution for $^{[6]}Al$ (Fig. 4A). The degree of $^{[6]}Al$ substitution is similar among these illite samples, but those from Centennial and Maurice Bay are the most K deficient (Fig. 4A). Illite from all five studied alteration systems plots within the typical compositional range for illite (Rieder et al., 1998; Rosenberg, 2002). Formation temperatures for illite from the Centennial deposit (ca. 180 °C) are lower than those from Wheeler River Zone "K", McArthur River Zone 4, Maurice Bay, and Spring Point, which formed under a relatively restricted range of temperatures from 220–240 °C (Table 1).

Chlorite from the five studied sandstone-hosted alteration systems occurs as the di-trioctahedral variety, with trioctahedral chlorite also present at the apparently barren Wheeler River Zone "K" system. Di-trioctahedral chlorite samples are compositionally and mineralogically similar to sudoite and contain Al_2O_3 contents between 27.3 and 35.1 wt.% but variable MgO and FeO_T contents (Fig. 4B; Table 1). The typical range of MgO content varies from 10.2 to 14.6 wt.%, with the exception of sudoite from Centennial, which are poorer in Mg and have ca. 6.0 wt.% MgO. Typical Fe contents range from 0.5 to 3.5 wt.% FeO_T, with the exception of C2 sudoite at McArthur River Zone 4, which has greater Fe contents (ca. 9.1 wt.% FeO_T). Sudoite samples from these systems have $^{[4]}Al$ ranging from 0.21 to 0.71, $^{[6]}Al$ from 2.46 to 3.37, $^{[6]}Mg$ from 0.83 to 1.91, and total occupancy of octahedrally coordinated sites of 4.34 to 4.87 apfu (Fig. 4B); these values are within the normal range for sudoite (Bailey and Lister, 1989). Trioctahedral chlorite at Wheeler River Zone "K" has Al_2O_3, MgO, and FeO_T contents of 19.2 wt.%, 21.8 wt.%, and 7.4 wt.%, respectively, and is compositionally similar to clinochlore (Fig. 4B). This clinochlore has a total octahedral occupancy of 5.56 cations per six octahedrally coordinated sites, which is less than the ideal number, indicating minor dioctahedral substitution (Table 1). Based on $^{[4]}Al$ occupancy, sudoite formation temperatures typically range from 150 to 175 °C, with the exception of sudoite from Centennial which has slightly higher formation temperatures of around 200 °C (Table 1). Clinochlore at Wheeler River Zone "K" records higher formation temperatures (ca. 230 °C) than sudoite and are similar to the formation temperatures for illite (Table 1). Late pre-ore sudoite from each system records relatively lower formation temperatures than illite, which most likely reflects the inaccuracy of the empirical chlorite geothermometers when applied to di-trioctahedral chlorite (e.g. sudoite) since they were calibrated using trioctahedral chlorite varieties.

4.3. Alteration patterns in sandstone-hosted alteration systems

Alteration within the five sandstone-hosted systems consists of diagenetic kaolinite (e.g. Maurice Bay, Spring Point, Centennial) or dickite (e.g. McArthur River Zone 4, Wheeler River Zone "K") overprinted by zones of dravite, illite, sudoite, clinochlore, and late kaolinite alteration surrounding the faulted unconformity (Figs. 5–9). Illite typically forms a wider, more spatially-extensive, zone of alteration in the peripheral region of the alteration system. At McArthur River Zone 4, the occurrence of illite and illite–chlorite mixed layer (ICML) clay delineates a 300 m-high by 350 m-wide zone above the Zone 4 ore body (Fig. 5). Similarly at the barren Wheeler River Zone "K" system, illite alteration occurs up to 400 m above the unconformity and extends several kilometers outside of the Zone "K" trend (Fig. 6). Sudoite and clinochlore alteration occurs near the center of these sandstone-hosted systems but varies in extent. Mineralized systems at McArthur River Zone 4 and Maurice Bay seem to have smaller sudoite halos compared to the sudoite and clinochlore halos in the barren systems at Wheeler River Zone "K" and Spring Point. At McArthur River Zone 4, two sudoite alteration zones are present (Fig. 5). C1 Mg-rich sudoite associated with diagenesis predominates within a 50–100 m-thick horizon near the MFc–MFd boundary, whereas, C2 Mg–Fe-rich sudoite associated with hydrothermal alteration delineates a 50 m-high by 100 m-wide halo straddling the faulted unconformity. At Centennial, the occurrence of

Table 1
Average chemical composition (and 1σ) and formation temperatures of pre-ore illite and chlorite from sandstone-hosted alteration systems.

Oxide wt. %											Analytical total (%)	Formation temp. (°C)	$Fe^{3+}/\Sigma Fe$ median	Mineral formula
SiO_2	TiO_2	Al_2O_3	FeO_T[a]	MnO	MgO	CaO	Na_2O	K_2O	Cl	F				
Illite														
Wheeler River Zone K (basin)														
48.1 ± 1.4	<DL	33.2 ± 1.2	1.2 ± 0.8	<DL	1.0 ± 0.3	0.1 ± 0.1	0.1 ± 0.1	9.3 ± 0.7	n.a.	n.a.	93.2	240	1.00	$K_{0.80}Mg_{0.10}Fe^{3+}_{0.07}Al_{1.85}[Si_{3.23}Al_{0.77}O_{10}](OH)_2$
Spring Point (basin)														
47.55 ± 0.48	<DL	31.62 ± 0.39	1.66 ± 0.22	<DL	1.70 ± 0.15	0.10 ± 0.15	0.13 ± 0.02	9.47 ± 0.14	n.a.	n.a.	92.28	230	n.a.	$K_{0.83}Mg_{0.10}Fe^{2+}_{0.04}Al_{1.91}[Si_{3.21}Al_{0.77}O_{10}](OH)_2$
Maurice Bay (basin)														
47.99 ± 0.34	<DL	34.07 ± 0.24	0.45 ± 0.03	<DL	0.95 ± 0.02	0.13 ± 0.01	0.12 ± 0.01	8.38 ± 0.08	n.a.	n.a.	92.19	220	n.a.	$K_{0.72}Mg_{0.10}Fe^{2+}_{0.03}Al_{1.90}[Si_{3.21}Al_{0.80}O_{10}](OH)_2$
Centennial (basin)														
51.63 ± 4.56	<DL	26.23 ± 1.74	0.73 ± 0.16	<DL	0.73 ± 0.15	0.25 ± 0.12	0.18 ± 0.1	7.51 ± 0.65	n.a.	n.a.	87.54	180	n.a.	$K_{0.67}Mg_{0.08}Fe^{2+}_{0.04}Al_{1.80}[Si_{3.63}Al_{0.37}O_{10}](OH)_2$
McArthur River Zone 4 (basin)														
45.68 ± 2.13	0.02 ± 0.01	32.94 ± 0.81	0.77 ± 0.15	0.02 ± 0.01	0.48 ± 0.11	0.06 ± 0.01	0.04 ± 0.02	8.83 ± 0.55	0.02 ± 0.01	0.21 ± 0.09	89.04	235	1.00	$K_{0.79}Mg_{0.05}Fe^{3+}_{0.05}Al_{1.92}[Si_{3.20}Al_{0.80}O_{10}](OH_{1.95}F_{0.05})$
Sudoite														
Wheeler River Zone K (basin)														
33.5 ± 5.4	<DL	28.2 ± 5.0	1.4 ± 0.7	<DL	10.2 ± 3.3	0.1 ± 0.1	0.1 ± 0.1	1.1 ± 0.9	n.a.	n.a.	86.2	175	0.37	$\square_{1.34}Mg_{1.58}Fe^{2+}_{0.08}Fe^{3+}_{0.05}Al_{2.95}(Si_{3.49}Al_{0.51})O_{10}(OH)_8$
Spring Point (basin)														
37.35 ± 0.26	<DL	35.05 ± 0.25	0.48 ± 0.04	<DL	14.57 ± 0.10	0.10 ± 0.01	0.04 ± 0.01	0.24 ± 0.01	n.a.	n.a.	87.91	170	0.36	$\square_{1.13}Mg_{1.91}Fe^{2+}_{0.02}Fe^{3+}_{0.01}Al_{2.92}(Si_{3.29}Al_{0.71})O_{10}(OH)_8$
Maurice Bay (basin)														
37.43 ± 0.62	<DL	33.50 ± 0.54	3.50 ± 0.14	<DL	12.37 ± 0.42	0.17 ± 0.04	0.03 ± 0.01	1.24 ± 0.20	n.a.	n.a.	88.27	150	0.55	$\square_{1.25}Mg_{1.64}Fe^{2+}_{0.12}Fe^{3+}_{0.14}Al_{2.85}(Si_{3.33}Al_{0.67})O_{10}(OH)_8$
Centennial (basin)														
40.96 ± 4.30	<DL	32.80 ± 5.95	1.84 ± 0.84	<DL	6.00 ± 3.70	0.25 ± 0.11	0.12 ± 0.12	0.23 ± 0.34	n.a.	n.a.	84.92	200	0.36	$\square_{1.66}Mg_{0.83}Fe^{2+}_{0.09}Fe^{3+}_{0.05}Al_{3.37}(Si_{3.79}Al_{0.21})O_{10}(OH)_8$
McArthur River Zone 4 (C1, basin)														
35.99 ± 0.95	<DL	31.78 ± 1.02	0.68 ± 0.22	0.01 ± 0.01	10.36 ± 0.37	0.10 ± 0.03	0.05 ± 0.04	1.16 ± 0.12	0.02 ± 0.01	0.20 ± 0.14	80.36	160	0.93	$\square_{1.38}Mg_{1.49}Fe^{2+}_{0.00}Fe^{3+}_{0.05}Al_{3.07}(Si_{3.47}Al_{0.53})O_{10}(OH_{7.94}F_{0.06})$
McArthur River Zone 4 (C2, basin)														
34.74 ± 2.55	0.02 ± 0.02	27.28 ± 3.78	9.12 ± 5.87	0.03 ± 0.03	11.65 ± 2.11	0.31 ± 0.08	0.05 ± 0.04	0.29 ± 0.11	0.17 ± 0.05	0.31 ± 0.21	83.96	155	0.45	$\square_{1.13}Mg_{1.68}Fe^{2+}_{0.40}Fe^{3+}_{0.33}Al_{2.46}(Si_{3.35}Al_{0.65})O_{10}(OH_{7.88}F_{0.09}Cl_{0.03})$
Clinochlore														
Wheeler River Zone K (basin)														
29.8 ± 2.5	<DL	19.2 ± 2.9	7.4 ± 1.1	<DL	21.8 ± 2.7	0.1 ± 0.1	<DL	0.1 ± 0.1	n.a.	n.a.	82.8	230	0.34	$\square_{0.44}Mg_{3.41}Fe^{2+}_{0.43}Fe^{3+}_{0.22}Al_{1.50}(Si_{3.13}Al_{0.87})O_{10}(OH)_8$

NOTES: n.a. = not analyzed; <DL = below detection limit. Standard deviation given as 1σ. Abbreviations: bsmt = basement, □ = vacancy.
[a] Total Fe expressed as FeO.

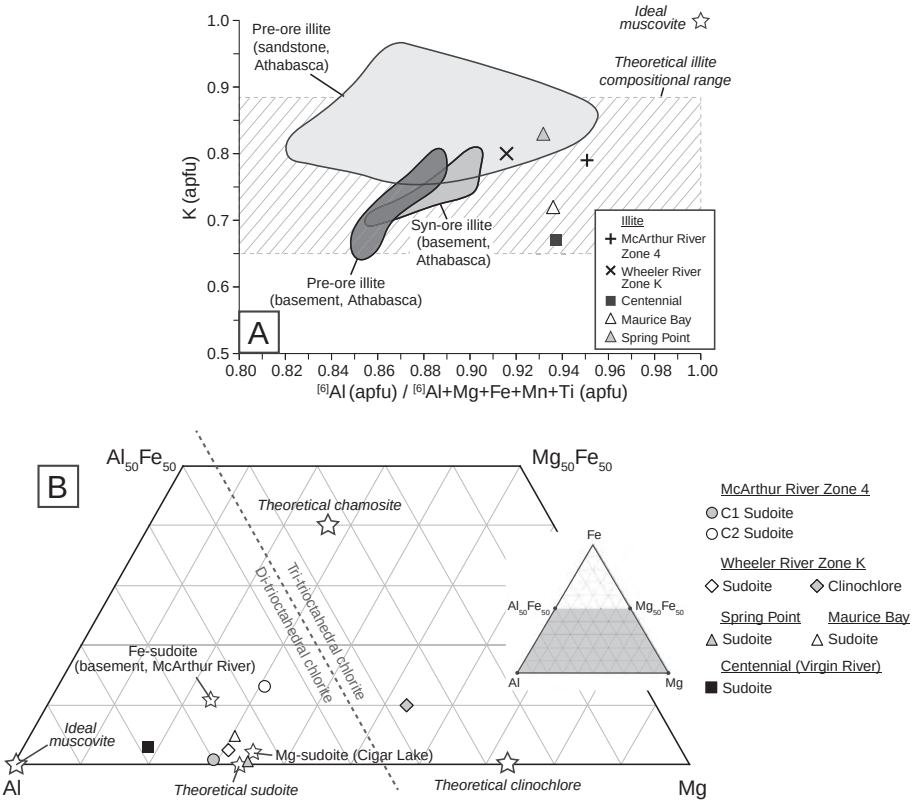

Fig. 4. A. Plot of K interlayer site occupancy versus the extent of substitution for octahedral Al in illite from sandstone-hosted alteration systems. B. Molar Fe–Al–Mg ternary plot for chlorite from sandstone-hosted alteration systems. Composition for minerals from Athabasca Basin deposits and the theoretical composition of major mineral species are indicated (data from Alexandre et al., 2005; Bailey and Lister, 1989; Billault et al., 2002; Cloutier et al., 2009, 2011; Percival and Kodama, 1989; Percival et al., 1993; Wilson and Kyser, 1987; Wilson et al., 1987).

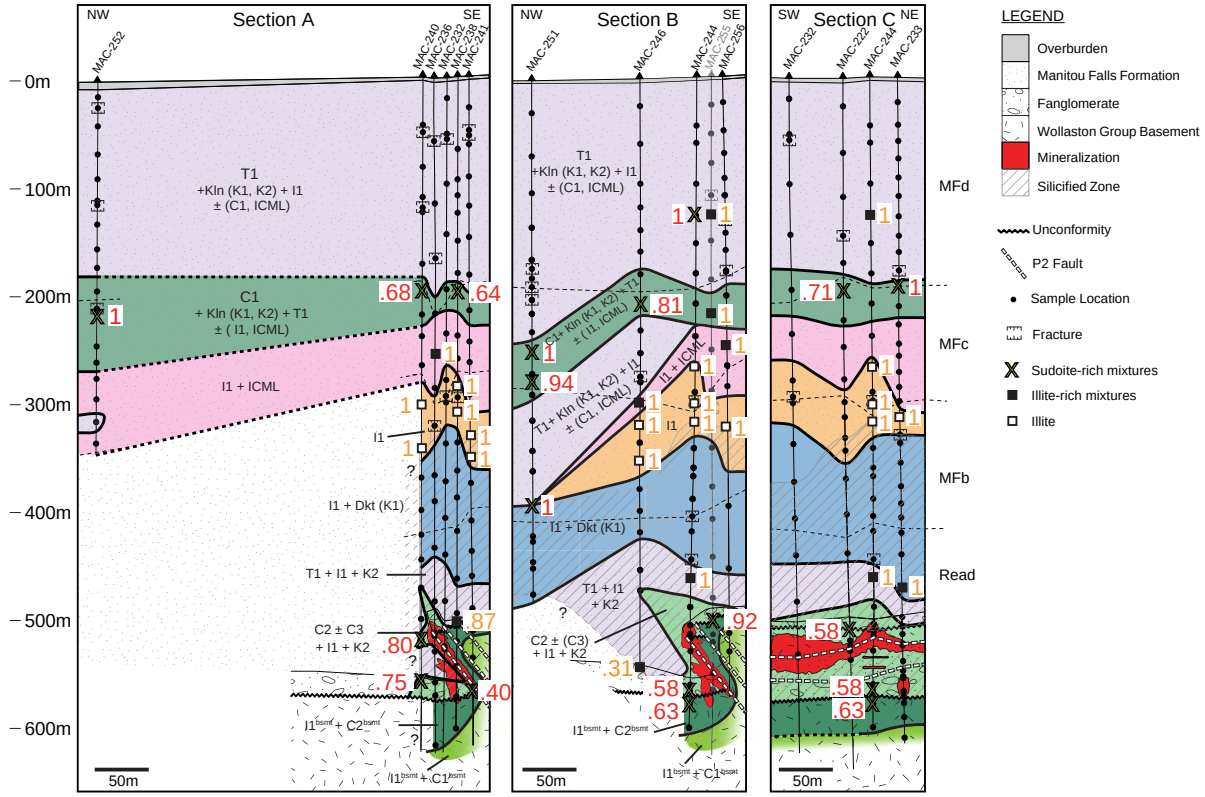

Fig. 5. Longitudinal cross-sections of McArthur River Zone 4 showing the spatial distribution and $Fe^{3+}/\Sigma Fe$ ratios of alteration minerals. Drill hole MAC-255 is projected onto section B. Abbreviation for pre-ore minerals: C1 = Mg-rich sudoite, T1 = magnesiofoititte, K1 = dickite (dkt), kaolinite (kln), I1 = illite, $I1^{bsmt}$ = illite in basement, $C1^{bsmt}$ = clinochlore in basement, C2 = Mg–Fe-rich sudoite, $C2^{bsmt}$ = Mg-rich sudoite in basement, ICML = illite–chlorite mixed layer clay; syn-ore minerals: C3 = Fe–Mg-rich sudoite; post-ore minerals: K2 = post-ore kaolinite.

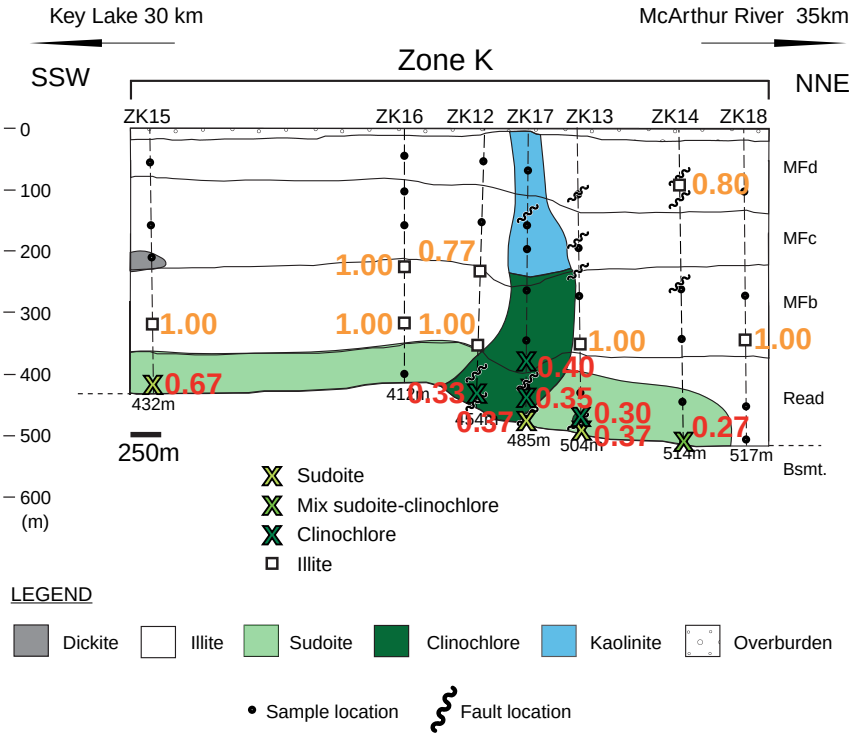

Fig. 6. Longitudinal cross-section of the Wheeler River Zone "K" area along a south-southwest to north-northeast transect, showing major lithological units, structures, and position of drill core samples (modified after Cloutier et al., 2010). The spatial distribution of alteration minerals within the Read and Manitou Falls Formations and $Fe^{3+}/\Sigma Fe$ values of clay separates are indicated.

sudoite in drill hole VR-04 suggests that sudoite alteration extends at least 240 m from the deposit and 200 m above the unconformity (Fig. 7). Sudoite alteration at the Maurice Bay deposit forms a narrow 20 m-high by 135 m-wide zone above the faulted unconformity (Fig. 8). At Wheeler River Zone "K", sudoite alteration demarcates a 100 m-high by 4 km-wide halo along the basal Read Formation and is overprinted by a 250 m-high by 500 m-wide clinochlore halo above the basement shear zone (Fig. 6). Similarly at Sprint Point, a spatially-extensive sudoite halo measuring 150 m-high by more than 2 km-wide extends along the base of the Fair Point Formation (Fig. 9).

4.4. Stable isotope geochemistry

The oxygen and hydrogen isotopic compositions and formation temperatures for the illite, sudoite, and clinochlore samples analyzed by Mössbauer spectroscopy are tabulated in Table 2. These values

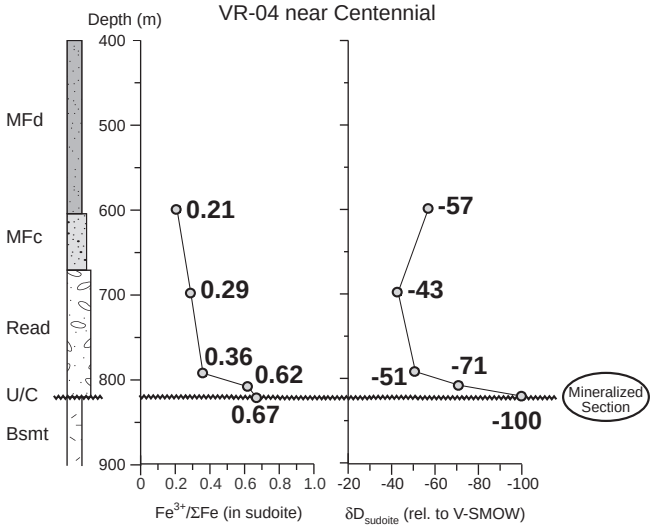

Fig. 7. Downhole plot of $Fe^{3+}/\Sigma Fe$ ratios and δD values of sudoite in drill hole VR-04 proximal to the Centennial deposit. The $Fe^{3+}/\Sigma Fe$ ratio of sudoite increases towards the weakly mineralized unconformity.

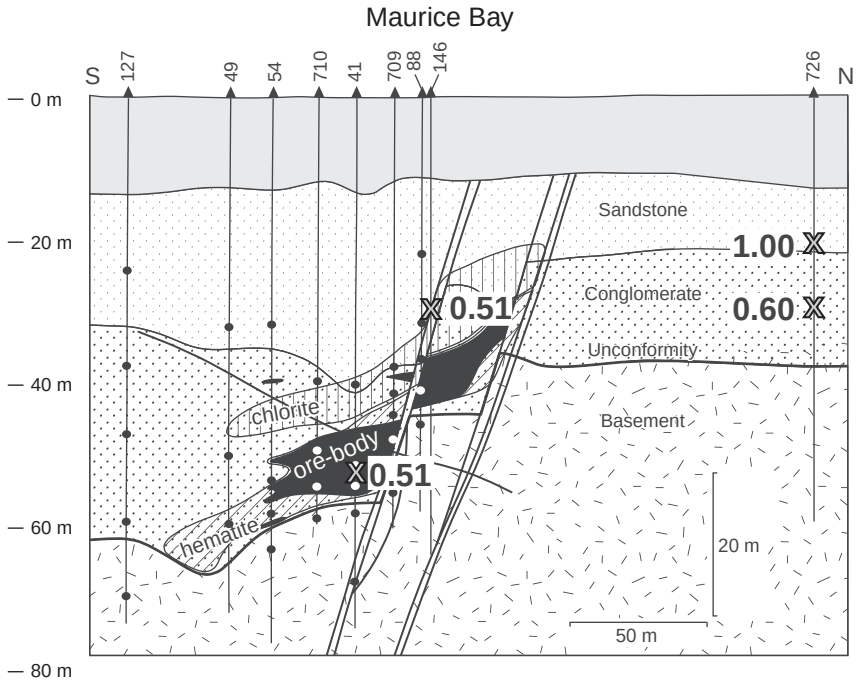

Fig. 8. Longitudinal cross-section of the Maurice Bay Main ore body along a north–south-oriented transect (modified after Alexandre et al., 2009a). Major lithological units, structures, drill holes and drill core samples, key alteration zones, and $Fe^{3+}/\Sigma Fe$ ratios of sudoite are indicated.

should reflect fluid conditions during the formation of these minerals or subsequent interactions with recent post-formational fluids (Kotzer and Kyser, 1995; Wilson and Kyser, 1987). The calculated isotopic compositions of the fluid in equilibrium with these minerals are plotted in Fig. 10.

Pre-ore illite samples from the barren Wheeler River Zone "K" and mineralized McArthur River Zone 4 systems have $\delta^{18}O$ values near 10‰ but more variable δD values from −91 to −37‰ (Table 2). The majority of illite from Wheeler River Zone "K" and McArthur River Zone 4 has δD values above −70‰. Illite–ICML mixtures from McArthur River Zone 4 have similar isotopic compositions as illite (Table 2). The presence of dickite or kaolinite in the illite samples shifts the isotopic composition towards higher $\delta^{18}O$ and lower δD values.

As illite samples from McArthur River Zone 4 and Wheeler River Zone "K" have similar oxygen isotopic compositions and temperatures of formation, their calculated fluid compositions are similar (Fig. 10; Table 2). However, the δD values of the fluid producing illite at McArthur River Zone 4 is lower than that at Wheeler River Zone "K", although both fluids are comparable with basinal fluids in equilibrium with illite, dickite, and kaolinite alteration in other deposits of the Athabasca Basin (Fig. 10).

The oxygen and hydrogen isotopic compositions of late pre-ore sudoite from the five sandstone-hosted alteration systems are similar, with values typically ranging from +7.0 to +10.4‰ and −72 to −43‰, respectively (Table 2). Sudoite from drill hole VR-04 near Centennial defines two isotopically-distinct groups, with one

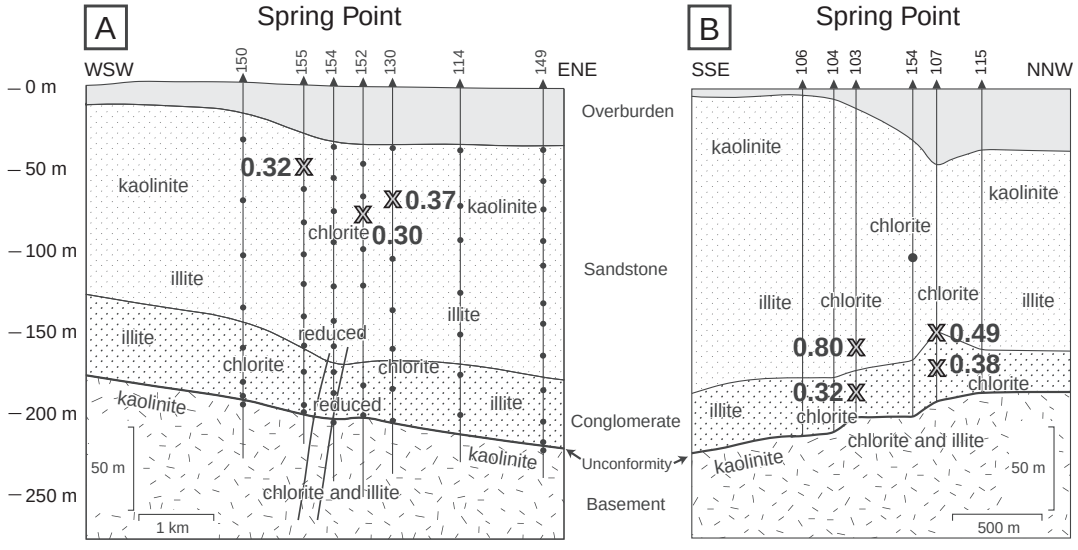

Fig. 9. Longitudinal cross-sections of the barren Spring Point alteration system along a west-southwest to east-northeast (A) and south-southeast to north-northwest (B) transect (modified after Alexandre et al., 2009a). Major lithological units, drill holes and core sample locations, spatial distribution of alteration minerals, and $Fe^{3+}/\Sigma Fe$ ratio of sudoite are indicated.

Table 2
Oxygen and hydrogen stable isotopic composition of alteration minerals from sandstone-hosted alteration systems.

Sample DDH-depth (m)	Lithology	Mineralogy %	Size fraction μm	Mineral		Formation temp. (°C)	Fluid	
				$\delta^{18}O$	δD		$\delta^{18}O$	δD
				(‰ rel. V-SMOW)			(‰ rel. V-SMOW)	
McArthur River Zone 4								
Pre-ore illite								
MAC233-315	MFb	100 I	1–2	12.7	−78	235	8.1	−64
MAC238-287	MFb	100 I	1–2	9.4	−73	235	4.8	−59
MAC238-311	MFb	100 I	1–2	11.1	−66	235	6.5	−52
MAC240-302	MFb	100 I	1–2	10.3	−60	235	5.7	−46
MAC240-344	MFb	100 I	1–2	12.1	−62	235	7.5	−48
MAC241-333	MFb	100 I	1–2	10.9	−73	235	6.3	−60
MAC241-353	MFb	100 I	1–2	10.6	−64	235	6.0	−50
MAC244-269	MFc	100 I	1–2	9.8	−70	235	5.2	−57
MAC244-303	MFc	100 I	1–2	11.0	−65	235	6.4	−51
MAC244-320	MFb	100 I	1–2	10.4	−91	235	5.8	−77
MAC246-320	MFb	100 I	1–2	9.6	−67	235	5.0	−53
MAC246-354	MFb	100 I	1–2	11.2	−63	235	6.6	−49
MAC256-325	MFb	100 I	1–2	11.0	−62	235	6.4	−48
Pre-ore illite and ICML								
MAC236-256	MFc	70 I, 30 ICML	1–2	9.4	−60	235	–	–
MAC246-300	MFc	70 I, 30 ICML	1–2	11.4	−63	235	–	–
MAC256-249	MFc	40 I, 60 ICML	1–2	11.3	−62	235	–	–
Pre-ore illite and dickite								
MAC233-473	Read	20 I, 80 Dkt	<2	13.2	−96	–	–	–
MAC244-464	Read	50 I, 40 Dkt, 10 Q	2–5	12.1	−78	–	–	–
Pre-ore illite and post-ore kaolinite								
MAC238-505	HW FAN	35 I, 65 K	2–5	9.9	−106	–	–	–
MAC246-545	FW FAN	90 I, 10 K	<2	12.3	−74	–	–	–
Pre-ore C1 Mg-sudoite								
MAC222-197	MFc	20 I, 20 C1, 10 K, 50 Dr	1–2	9.7	−58	–	–	–
MAC233-194	MFc	10 I, 25 C1, 30 K, 35 Dr	2–5	9.2	−83	–	–	–
MAC238-199	MFc	20 I, 10 C1, 10 K, 60 Dr	2–5	12.4	−80	–	–	–
MAC240-197	MFc	10 I, 40 C1, 20 K, 30 Dr	2–5	10.7	−73	–	–	–
MAC246-209	MFc	35 I, 35 ICML, 10 C1, 15 Dr	<1	10.2	−73	–	–	–
MAC251-252	MFc	10 I, 50 C1, 25 K, 10 Dr	1–2	8.8	−61	–	–	–
MAC251-279	MFc	75 C1, 20 K, 5 Dr	1–2	12.5	−57	–	–	–
MAC251-393	MFb	55 I, 10 C1, 25 Dkt, 10 Q	5–10	11.9	−53	–	–	–
MAC252-215	MFc	65 C1, 35 K	1–2	10.5	−62	–	–	–
MAC255-220	MFc	70 I, 15 C1, 5 K, 5 Dr, 5 Q	2–5	12.5	−76	–	–	–
C1 sud		100 C1 (upper limit)	–	8.5	−45	160	4.9	−43
C1 sud		100 C1 (lower limit)	–	7.7	−70	160	4.1	−68
Pre-ore C2 Mg–Fe sudoite (alteration halo)								
MAC222-509	HW FAN	95 C2, 5 I	1–2	9.6	−106	–	–	–
MAC240-521	MFa	10 I, 40 C2, 45 K, 5 Dr	1–2	10.1	−91	–	–	–
MAC240-560	FW FAN	45 I, 55 C2	1–2	8.9	−53	–	–	–
MAC241-569	BSMT	100 C2	<2	7.8	−56	–	–	–
MAC244-569	FW FAN	55 C2, 35 I, 5 Dr, 5 Q	1–2	9.0	−61	–	–	–
MAC244-581	BSMT	60 I, 40 C2	1–2	8.1	−49	–	–	–
MAC255-504	HW FAN	10 I, 65 K, 25 C2	2–5	10.2	−108	–	–	–
C2 sud		100 C2 (upper limit)	–	8.7	−50	155	4.9	−25
C2 sud		100 C2 (lower limit)	–	7.7	−65	155	3.9	−40
Wheeler River Zone K								
Pre-ore illite								
ZK12-242	MFb	100 I	<2	11.6	−37	240	7.2	−24
ZK12-360	MFb	100 I	<2	9.4	−38	240	5.0	−25
ZK13-352	MFb	100 I	<2	10.6	−48	240	6.2	−35
ZK14-100	MFd	100 I	<2	11.0	−62	240	6.6	−49
ZK15-325	MFb	100 I	<2	10.7	−53	240	6.3	−40
ZK16-320	MFb	100 I	<2	9.8	−58	240	5.4	−45
ZK18-351	MFb	100 I	<2	10.5	−44	240	6.1	−31
Pre-ore sudoite								
ZK15-425	Read	100 Sud	<2	10.4	−59	175	7.3	−54
Pre-ore clinochlore								
ZK12-430	Read	100 Cln	<2	6.3	−37	230	4.8	−23
ZK13-480	Read	100 Cln	<2	3.0	−46	230	1.5	−32
ZK17-381	MFb	100 Cln	<2	5.6	−54	230	4.1	−40
ZK17-426	Read	100 Cln	<2	3.0	−43	230	1.5	−29
Spring Point								
Pre-ore sudoite								
SN103-159	FP SS	100 Sud	n.a.	8.3	−55	170	5.1	−54
SN107-149	FP Cong.	100 Sud	n.a.	8.9	−47	170	5.7	−46
SN107-149dup	FP Cong.	100 Sud	n.a.	8.9	−51	170	5.7	−50
SN107-171a	FP Cong.	100 Sud	n.a.	9.4	−46	170	6.2	−45
SN107-171dup	FP Cong.	100 Sud	n.a.	9.4	−46	170	6.2	−45

Table 2 (*continued*)

Sample DDH-depth (m)	Lithology	Mineralogy %	Size fraction μm	Mineral		Formation temp. (°C)	Fluid	
				$\delta^{18}O$	δD		$\delta^{18}O$	δD
				(‰ rel. V-SMOW)			(‰ rel. V-SMOW)	
Pre-ore sudoite	FP SS	100 Sud	n.a.	7.8	−51	170	4.6	−50
SN152-71	FP SS	100 Sud	n.a.	8.6	−49	170	5.4	−48
SN155-54	FP SS	100 Sud	n.a.	8.3	−48	170	5.1	−47
SN155-54dup	FP SS	100 Sud	n.a.	8.3	−46	170	5.1	−45
Maurice Bay								
Pre-ore sudoite								
MB726-20	–	100 Sud	n.a.	9.6	−72	150	5.6	−61
MB726-29	–	100 Sud	n.a.	11.1	−62	150	7.1	−51
Centennial								
Pre-ore sudoite								
VR04-599	MFd	100 Sud	n.a.	8.7	−57	200	6.4	−45
VR04-698	Read	100 Sud	n.a.	8.0	−43	200	5.7	−31
VR04-792	Read	100 Sud	n.a.	7.0	−51	200	4.7	−39
VR04-808	Read	100 Sud	n.a.	11.5	−71	200	9.2	−59
VR04-821	Read	100 Sud	n.a.	11.7	−100	200	9.4	−88

Lithology abbreviations: FP = Fair Point Formation, MF = Manitou Falls Formation, FW = footwall, HW = hanging wall, SS = sandstone, Cong = conglomerate, FAN = fanglomerate, BSMT = basement. Mineralogy abbreviations: I = illite, ICML = illite–chlorite mixed layer clay, Cln = clinochlore K = kaolinite, Dkt = dickite, Sud = sudoite, C1 = Mg sudoite, C2 = Mg–Fe sudoite, Dr = dravite, Q = quartz, n.a. = not available.

having $\delta^{18}O$ values between +7.0 and +8.7‰ and δD values between −57 and −43‰ and the second, represented by the two sudoite samples near the unconformity, with higher $\delta^{18}O$ (= +11.5 to +11.7‰) and lower δD (= −100 to −71‰) values. Both pre-ore diagenetic C1 sudoite and hydrothermal C2 sudoite from McArthur River Zone 4 have similar $\delta^{18}O$ (+7.7 to +8.7‰) and δD (−70 to −45‰) values. Clinochlore samples from Wheeler River Zone "K" have similar hydrogen isotopic compositions as sudoite (δD = −54 to −37‰) but are more depleted in ^{18}O ($\delta^{18}O$ = +3.0 to +6.3‰).

Using formation temperatures defined in Table 2, fluids in equilibrium with sudoite from the studied alteration systems have $\delta^{18}O$ fluid values that typically range between +3.9 and +7.3‰ and δD fluid values that vary from −88 to −23‰, with most between −68 and −23‰ (Fig. 10; Table 2). The fluid in equilibrium with clinochlore at Wheeler River Zone "K" has distinctively lower $\delta^{18}O$ values than fluids producing sudoite indicating that the latter may have originated from deeper parts of the basement, according to Cloutier et al. (2010). The fluid producing the two sudoite samples near the unconformity at Centennial VR-04 has the highest $\delta^{18}O$ values (Fig. 10). C2 sudoite separates from the hydrothermal alteration halo at McArthur River Zone 4 are slightly more enriched in ^{2}H than diagenetic C1 sudoite in MFc and MFd (Fig. 10). The δD value of the fluid in equilibrium with C1 sudoite is within the range for basinal fluids forming illite at McArthur River Zone 4, suggesting that the lower δD value of C1 sudoite is not the result of a greater isotopic exchange with post-crystallization ^{2}H-depleted fluids.

4.5. Pb isotopic composition of weak-acid leachates

The $^{207}Pb/^{206}Pb$ ratios of leachable Pb from crushed drill cores, from which clay separates were analyzed by Mössbauer spectroscopy, are

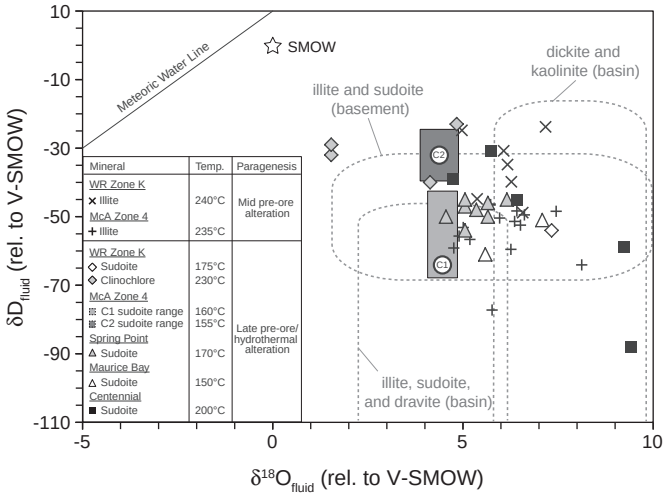

Fig. 10. $\delta^{18}O$ versus δD for fluids in equilibrium with illite and chlorite from studied sandstone-hosted alteration systems. Shaded boxes represent the range of fluid $\delta^{18}O$ and δD compositions corresponding to C1 and C2 sudoites from McArthur River Zone 4. Fluids in equilibrium with typical Athabasca Basin alteration minerals are indicated for reference (gray, dashed lines) (data from Alexandre et al., 2005; Cloutier et al., 2009; Kotzer and Kyser, 1995; Percival et al., 1993; Wasyliuk, 2001). Abbreviations: MWL = meteoric water line, SMOW = standard mean ocean water.

Table 3
Fe^{2+} and Fe^{3+} relative abundances (%) in clay separates determined by Mössbauer spectroscopy and leachable $^{207}Pb/^{206}Pb$ ratios in drill core.

Sample DDH-depth (m)	Size μm	Mineralogy (XRD) %	Fe^{3+} QSD site %	Fe^{3+} HFD site %	Total Fe^{3+} %	Total Fe^{2+} %	$Fe^{3+}/\Sigma Fe$ (in clay)	$^{207}Pb/^{206}Pb$ (leachate)	Distance to fault/ore body (m)
McArthur River Zone 4									
Pre-ore illite									
MAC233-315	1–2	100 I	10	90	100	–	1.00	0.837	–
MAC238-287	1–2	100 I	39	61	100	–	1.00	0.845	–
MAC238-311	1–2	100 I	39	61	100	–	1.00	0.812	–
MAC240-302	1–2	100 I	41	59	100	–	1.00	0.848	–
MAC240-344	1–2	100 I	36	64	100	–	1.00	0.863	–
MAC241-333	1–2	100 I	10	90	100	–	1.00	0.745	–
MAC241-353	1–2	100 I	14	86	100	–	1.00	0.851	–
MAC244-269	1–2	100 I	45	55	100	–	1.00	0.839	–
MAC244-303	1–2	100 I	38	62	100	–	1.00	0.858	–
MAC244-320	1–2	100 I	6	94	100	–	1.00	0.811	–
MAC246-320	1–2	100 I	61	39	100	–	1.00	0.89	–
MAC246-354	1–2	100 I	11	89	100	–	1.00	0.8	–
MAC256-325	1–2	100 I	40	60	100	–	1.00	0.805	–
Pre-ore illite–ICML									
MAC236-256	1–2	70 I, 30 ICML	38	62	100	–	1.00	0.818	–
MAC244-128	1–2	40 I, 40 ICML, 15 K, 5 Dr	11	89	100	–	1.00	0.82	–
MAC246-300	1–2	70 I, 30 ICML	43	57	100	–	1.00	0.83	–
MAC255-128	1–2	40 I, 50 ICML, 5 K, 5 Dr	5	95	100	–	1.00	0.854	–
MAC256-249	1–2	40 I, 60 ICML	35	65	100	–	1.00	0.849	–
Pre-ore illite–dickite									
MAC233-473	5–10	40 I, 50 Dkt, 10 Q	15	85	100	–	1.00	0.64	–
MAC244-464	5–10	80 I, 5 Dkt, 15 Q	10	90	100	–	1.00	0.28	–
Pre-ore illite and post-ore kaolinite									
MAC238-505	5–10	40 I, 45 K, 5 Dr, 10 Q	87	–	87	13	0.87	0.342	–
MAC246-545	5–10	55 I, 40 K, 5 Q	4	87	91	9	0.31	0.8	–
Pre-ore C1 Mg-sudoite									
MAC222-197	1–2	20 I, 20 C1, 10 K, 50 Dr	71	–	71	29	0.71	0.826	321
MAC233-194	2–5	10 I, 25 C1, 30 K, 35 Dr	23	77	100	–	1.00	0.81	326
MAC238-199	2–5	20 I, 10 C1, 10 K, 60 Dr	25	61	86	14	0.64	0.804	342
MAC240-197	2–5	10 I, 40 C1, 20 K, 30 Dr	26	62	88	12	0.68	0.845	316
MAC246-209	1–2	35 I, 35 ICML, 10 C1, 15 Dr	81	–	81	19	0.81	0.87	309
MAC251-252	1–2	10 I, 50 C1, 25 K, 10 Dr	42	58	100	–	1.00	0.863	299
MAC251-279	1–2	75 C1, 20 K, 5 Dr	30	68	98	2	0.94	0.856	276
MAC251-393	5–10	55 I, 10 C1, 25 Dkt, 10 Q	13	87	100	–	1.00	0.452	189
MAC252-215	1–2	65 C1, 35 K	26	74	100	–	1.00	0.81	423
MAC255-220	2–5	70 I, 15 C1, 5 K, 5 Dr, 5 Q	62	38	100	–	1.00	0.85	332
Pre-ore C2 Mg–Fe sudoite (alteration halo)									
MAC222-509	1–2	95 C2, 5 I	31	47	78	22	0.58	0.0536	11
MAC240-521	1–2	10 I, 40 C2, 45 K, 5 Dr	49	39	88	12	0.80	0.381	11
MAC240-560	2–5	35 I, 50 C2, 10 Dr, 5 Q	15	80	95	5	0.75	0.776	26
MAC241-569	5–10	85 C2, 5 Dr, 10 Q	40	–	40	60	0.40	0.204	0
MAC244-569	1–2	55 C2, 35 I, 5 Dr, 5 Q	44	24	68	32	0.58	0.39	26
MAC244-581	1–2	60 I, 40 C2	40	37	77	23	0.63	0.563	37
MAC255-504	5–10	25 I,15 C2,55 K,5 Q	35	62	97	3	0.92	0.79	25
Wheeler River Zone K									
Pre-ore illite									
ZK12-242	<2	100 I	46	40	86	14	0.77	0.79	–
ZK12-360	<2	100 I	11	89	100	–	1.00	0.52	–
ZK13-352	2–5	100 I	25	75	100	–	1.00	0.67	–
ZK14-100	<2	100 I	80	–	80	20	0.80	0.57	–
ZK15-325	<2	100 I	41	59	100	–	1.00	0.36	–
ZK16-235	2–5	100 I	35	65	100	–	1.00	0.55	–
ZK16-320	<2	100 I	20	80	100	–	1.00	0.55	–
ZK18-351	2–5	100 I	20	80	100	–	1.00	0.59	–
Pre-ore sudoite									
ZK13-503	<2	100 Sud	28	24	52	48	0.37	n.a.	875
ZK15-425	2–5	100 Sud	67	–	67	33	0.67	0.25	2750
ZK17-483	<2	100 Sud	37	–	37	63	0.37	0.43	438
Pre-ore clinochlore									
ZK12-430	<2	100 Cln	33	–	33	67	0.33	0.34	29
ZK13-480	2–5	100 Cln	30	–	30	70	0.30	0.76	875
ZK17-381	2–5	100 Cln	40	–	40	60	0.40	n.a.	445
ZK17-426	<2	100 Cln	35	–	35	65	0.35	0.63	438
Pre-ore sudoite–clinochlore									
ZK14-514	2–5	Sud–Cln mix	27	–	27	73	0.27	0.56	1688
Spring Point									
Pre-ore sudoite									
SN103-159		100 Sud	80	–	80	20	0.80	0.62	317
SN103-185		100 Sud	26	18	44	56	0.32	0.66	315
SN107-149		100 Sud	49	–	49	51	0.49	0.65	138

Table 3 (*continued*)

Sample DDH-depth (m)	Size μm	Mineralogy (XRD) %	Fe^{3+} QSD site %	Fe^{3+} HFD site %	Total Fe^{3+} %	Total Fe^{2+} %	$Fe^{3+}/\Sigma Fe$ (in clay)	$^{207}Pb/^{206}Pb$ (leachate)	Distance to fault/ore body (m)
Pre-ore sudoite									
SN107-171a		100 Sud	30	22	52	48	0.38	n.a.	133
SN107-171dup		100 Sud	28	20	48	52	0.35	n.a.	133
SN130-83		100 Sud	37	–	37	63	0.37	0.60	880
SN152-71		100 Sud	30	–	30	70	0.30	0.64	494
SN155-54		100 Sud	32	–	32	68	0.32	0.55	302
Maurice Bay									
Pre-ore sudoite									
MB41-187		100 Sud	34	33	67	33	0.51	0.0770	0
MB146-107		100 Sud	42	18	60	40	0.51	n.a.	7
MB726-20		100 Sud	6	94	100	–	1.00	0.1135	92
MB726-29		100 Sud	31	48	79	21	0.60	0.1090	91
Centennial									
Pre-ore sudoite									
VR04-599		100 Sud	21	–	21	79	0.21	0.77	222
VR04-698		100 Sud	29	–	29	71	0.29	0.76	123
VR04-792		100 Sud	36	–	36	64	0.36	n.a.	29
VR04-808		100 Sud	62	–	62	38	0.62	0.24	13
VR04-821		100 Sud	67	–	67	33	0.67	0.21	0

Abbreviations: DDH = diamond drill hole, n.a. = not available. SS = sandstone, FAN = fanglomerate, BSMT = basement.
Minerals: I = illite, ICML = illite–chlorite mixed layer clay, Cln = clinochlore, K = kaolinite, Dkt = dickite, Sud = sudoite, C1 = Mg sudoite, C2 = Mg–Fe sudoite, Dr = dravite, Q = quartz.

shown in Table 3. The majority of sandstones from the C1 sudoite-bearing, illite-ICML, and illite-rich alteration zones above the silicified zone at McArthur River Zone 4 (Fig. 5) have non-radiogenic $^{207}Pb/^{206}Pb$ isotope ratios ($^{207}Pb/^{206}Pb$ = 0.69–0.89; avg. of 0.82) with the exception of one radiogenic sample with a $^{207}Pb/^{206}Pb$ ratio of 0.45 (Table 3). Radiogenic Pb is mostly confined to sandstones immediately overlying the ore body ($^{207}Pb/^{206}Pb$ = 0.28–0.64), in the basal fanglomerate ($^{207}Pb/^{206}Pb$ = 0.34–0.8), and in the C2 sudoite alteration halo surrounding the P2 fault ($^{207}Pb/^{206}Pb$ = 0.05–0.79, avg. of 0.47; Table 3). At Maurice Bay, drill core samples containing sudoite are highly radiogenic and have $^{207}Pb/^{206}Pb$ ratios ranging from 0.08 to 0.11 (avg. of 0.10) (Table 3). This is in agreement with their close proximity (<100 m) to the Maurice Bay Main ore body (Fig. 8).

Sandstone samples containing illite, sudoite, and clinochlore within the Wheeler River Zone "K" trend have $^{207}Pb/^{206}Pb$ ratios ranging from 0.25 to 0.79 (avg. of 0.54), with sandstones occurring proximal to the shear zone structure or near the unconformity in drill hole ZK15 being the most radiogenic (Fig. 6; Table 3). Correlations between radiogenic Pb isotope ratios with Ca, Sr, Pb, and P in drill cores from Zone "K" indicate that the radiogenic Pb signature was likely derived from the decay of U in detrital apatite grains within the sample, (cf. Cloutier et al., 2010), possibly exposed as a result of crushing (Holk et al., 2003).

Sandstones from drill hole VR-04 at Centennial become increasingly radiogenic with depth towards the weakly mineralized unconformity. $^{207}Pb/^{206}Pb$ ratios decrease from 0.77 (non-radiogenic), at a depth of about 600 m, to 0.21 (highly radiogenic) near the unconformity (Fig. 7; Table 3).

Sandstones from the sudoite alteration halo at Spring Point have uniform $^{207}Pb/^{206}Pb$ ratios ranging from 0.55 to 0.66 (avg. of 0.62) (Fig. 9; Table 3). Although Spring Point is a barren alteration system, the $^{207}Pb/^{206}Pb$ ratio of leachable Pb from the Fair Point Formation is still weakly radiogenic. This radiogenic Pb was likely derived in-situ from U-bearing detrital minerals, such as zircon, which is well-preserved within the sandstones at Spring Point (cf. Alexandre et al., 2012).

4.6. Fe oxidation state of alteration minerals

The abundance of structural Fe^{2+} and Fe^{3+} and calculated $Fe^{3+}/\Sigma Fe$ parameters for alteration minerals from each system is given in Table 3 and plotted spatially for each system (Figs. 5–9). The $Fe^{3+}/\Sigma Fe$ ratios range from 0.77 to 1.00 for illite, 0.21 to 1.00 for sudoite, and 0.30 to 0.40 for clinochlore (Table 3). Representative Mössbauer spectra for illite and sudoite are illustrated in Fig. 11.

4.6.1. Illite

At McArthur River Zone 4, illite (13 samples) from the illite-rich alteration horizon above the silicified zone contains only Fe^{3+} (Fig. 5; Table 3). Five samples of mixed illite–ICML clay and two illite–dickite samples give the same result (Fig. 5). Two mixed illite–kaolinite samples from the basal fanglomerate have $Fe^{3+}/\Sigma Fe$ ratios of 0.31 and 0.87, indicating elevated structural Fe^{2+} in illite near the unconformity (Fig. 5). Eight illite samples from the barren Wheeler River Zone "K" system have $Fe^{3+}/\Sigma Fe$ ratios between 0.77 and 1.00, with an average $Fe^{3+}/\Sigma Fe$ ratio of 0.95 (Fig. 6; Table 3). Thus, Fe in illite from both Wheeler River Zone "K" and McArthur River Zone 4 occurs predominantly as Fe^{3+}, but some illite samples from Zone "K" have greater contents of structural Fe^{2+}.

4.6.2. Chlorite

Pre-ore diagenetic C1 sudoite from McArthur River Zone 4 has upper and lower $Fe^{3+}/\Sigma Fe$ limits of 1.00 and 0.85, respectively, indicating the predominance of structural Fe^{3+} (Table 3). In contrast, late pre-ore hydrothermal C2 sudoite has upper and lower $Fe^{3+}/\Sigma Fe$ limits of 0.56 and 0.34, respectively, indicating the greater abundances of Fe^{2+} compared to C1 sudoite (Table 3).

Three hydrothermal sudoite samples from the barren Wheeler River Zone "K" system have an average $Fe^{3+}/\Sigma Fe$ ratio of 0.47, with one anomalous sudoite sample having a higher $Fe^{3+}/\Sigma Fe$ ratio (=0.67) than the others (Fig. 6; Table 3). This sudoite sample occurs in a distant drill hole (ZK15) located about 2.6 km from the Zone "K" shear zone (Fig. 6). Late-hydrothermal clinochlore from Zone "K" (4 samples), which follows sudoite paragenetically, has an average $Fe^{3+}/\Sigma Fe$ ratio of 0.35, similar to nearby sudoite samples (Fig. 6; Table 3).

Five sudoite specimens from drill hole VR-04, near the Centennial deposit, have an average $Fe^{3+}/\Sigma Fe$ ratio of 0.43 (Table 3). There is a trend of increasing $Fe^{3+}/\Sigma Fe$ ratio from 0.21 to 0.67 with depth, wherein the two sudoite samples near the unconformity have higher $Fe^{3+}/\Sigma Fe$ ratios of 0.62 and 0.67 (Fig. 7; Table 3).

At the Maurice Bay deposit, there is an average $Fe^{3+}/\Sigma Fe$ ratio of 0.65 for four sudoite samples (Table 3). Sudoite (2 samples) proximal to the ore zone (MB41, MB146) records lower $Fe^{3+}/\Sigma Fe$ ratios (ca. 0.51) than sudoite (2 samples) from distal drill hole, MB726, which has $Fe^{3+}/\Sigma Fe$ ratios of 0.60 and 1.00 (Fig. 8).

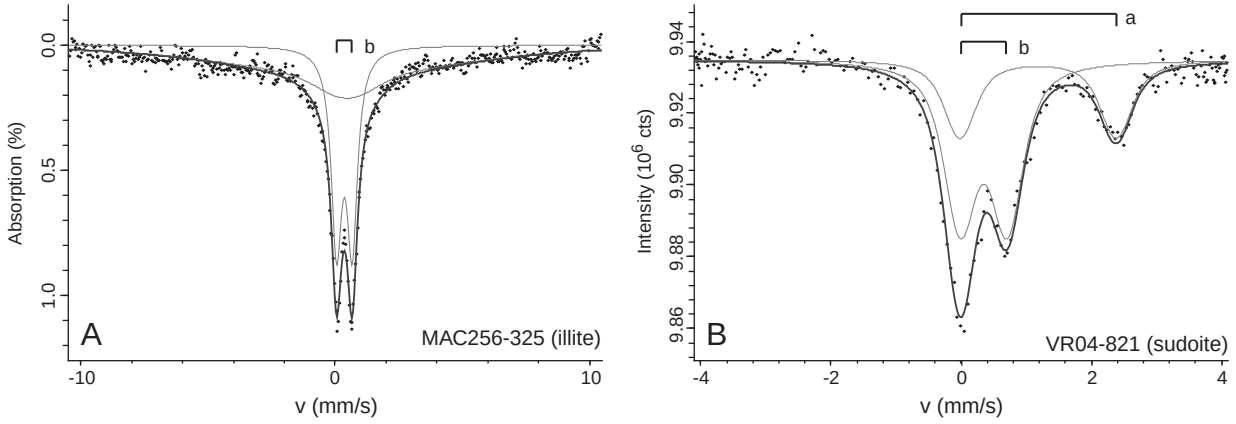

Fig. 11. Representative Mössbauer spectra for illite (A) and sudoite (B). Doublet "a" corresponds to octahedral Fe^{2+} and doublet "b" to octahedral Fe^{3+}. A. Illite from McArthur River Zone 4 containing octahedral Fe^{3+} with minor hematite (Fe^{3+}) broadened into a singlet near 0 mm/s. B. Sudoite from Centennial VR-04 containing both octahedral Fe^{2+} and octahedral Fe^{3+}.

Sudoite samples from the barren Spring Point alteration system have an average $Fe^{3+}/\Sigma Fe$ ratio of 0.42, with six samples having $Fe^{3+}/\Sigma Fe$ ratios between 0.30 and 0.49 and one outlier with a value of 0.80 (Fig. 9; Table 3). $Fe^{3+}/\Sigma Fe$ values of sudoite at Spring Point are relatively uniform and do not vary systematically with depth or proximity to the Spring Bay fault (Fig. 9).

4.6.3. Whole-rock

Mössbauer measurements on whole-rock samples from McArthur River Zone 4 were performed to determine whether whole-rocks would yield similar results to their corresponding clay separates. However, only one of the 12 whole-rock samples measured yielded sufficient absorption for the characterization of their $Fe^{3+}/\Sigma Fe$ ratios (Table 4). This sample (MAC241-569) also contained the highest modal abundance of sudoite in its clay fraction (ca. 85% C2 sudoite, 5% dravite, 10% quartz) (Table 3). The $Fe^{3+}/\Sigma Fe$ ratio of this whole-rock sample was 0.37, which is similar to the value of its corresponding clay separate ($Fe^{3+}/\Sigma Fe = 0.40$). Insufficient absorption was obtained for whole-rock samples in which illite was the predominant phyllosilicate and for whole-rock samples in which sudoite occurred with a high abundance of illite, kaolinite, or dravite. The application of whole-rock ^{57}Fe Mössbauer analysis to Athabasca Basin drill cores is limited by the low abundance, typically <10%, of clay minerals in the whole-rock, the low Fe concentration in alteration minerals, and the presence of hematite impurities (1–3%) that mask the absorption by phyllosilicates.

4.6.4. Comparison of $Fe^{3+}/\Sigma Fe$ ratios between alteration systems

Illite samples from Wheeler River Zone "K" have the same $Fe^{3+}/\Sigma Fe$ ratios as those from McArthur River Zone 4 ($Fe^{3+}/\Sigma Fe = 1$), with the exception of two illite specimens at Zone "K" which have $Fe^{3+}/\Sigma Fe$ ratios of 0.77 and 0.80, reflecting more reducing conditions (Fig. 12A). Chlorite samples from barren alteration halos (e.g. clinochlore and sudoite at Wheeler River Zone "K" and sudoite at Spring Point) and sudoite from the weakly-mineralized drill hole (VR-04) near the Centennial deposit have low median $Fe^{3+}/\Sigma Fe$ ratios between 0.3 and 0.4 (Fig. 12B). Chlorite from the alteration halos of mineralized systems (e.g. C2 sudoite at McArthur River Zone 4 and sudoite at Maurice Bay) is more oxidized and has higher median $Fe^{3+}/\Sigma Fe$ ratios between 0.45 and 0.55 (Fig. 12B).

5. Discussion

5.1. $Fe^{3+}/\Sigma Fe$ ratios in chlorite and the critical geochemical factor for U mineralization

Sandstone-hosted alteration systems in the Athabasca Basin are the result of interactions between high temperature diagenetic basinal fluids and reducing basement-derived fluids. The oxidation state of

Table 4
Fe^{2+} and Fe^{3+} relative abundances (%) in whole-rock from McArthur River Zone 4 by Mössbauer spectroscopy.

Sample DDH-depth (m)	Clay Mineralogy (XRD) %	Fe^{3+} QSD site %	Fe^{3+} HSD site %	Total Fe^{3+} %	Total Fe^{2+} %	$Fe^{3+}/\Sigma Fe$ (whole-rock)
Illite-bearing drill core (n = 7)						
MAC236-256	70 I, 30 ICML	–	–	–	–	No absorption
MAC240-344	100 I	–	–	–	–	No absorption
MAC240-447	57 I, 37 Dkt, 6 Q	–	–	–	–	No absorption
MAC240-560	45 I, 55 C2	–	–	–	–	No absorption
MAC241-333	100 I	–	–	–	–	No absorption
MAC241-440	18 I, 79 Dkt, 3 Q	–	–	–	–	No absorption
MAC252-294	15 Dr, 42 I, 43 ICML	–	–	–	–	No absorption
Chlorite-bearing drill core (n = 5)						
MAC238-199	20 I, 10 C1, 10 K, 60 Dr	–	–	–	–	No absorption
MAC240-197	10 I, 40 C1, 20 K, 30 Dr	–	–	–	–	No absorption
MAC240-521	10 I, 40 C2, 45 K, 5 Dr	–	–	–	–	No absorption
MAC241-569	85 C2, 5 Dr, 10 Q	37	–	37	63	0.37
MAC252-215	65 C1, 35 K	–	–	–	–	No absorption

Minerals: I = illite, ICML = illite–chlorite mixed layer clay, K = kaolinite, Dkt = dickite, C1 = Mg sudoite, C2 = Mg–Fe sudoite, Dr = dravite, Q = quartz.

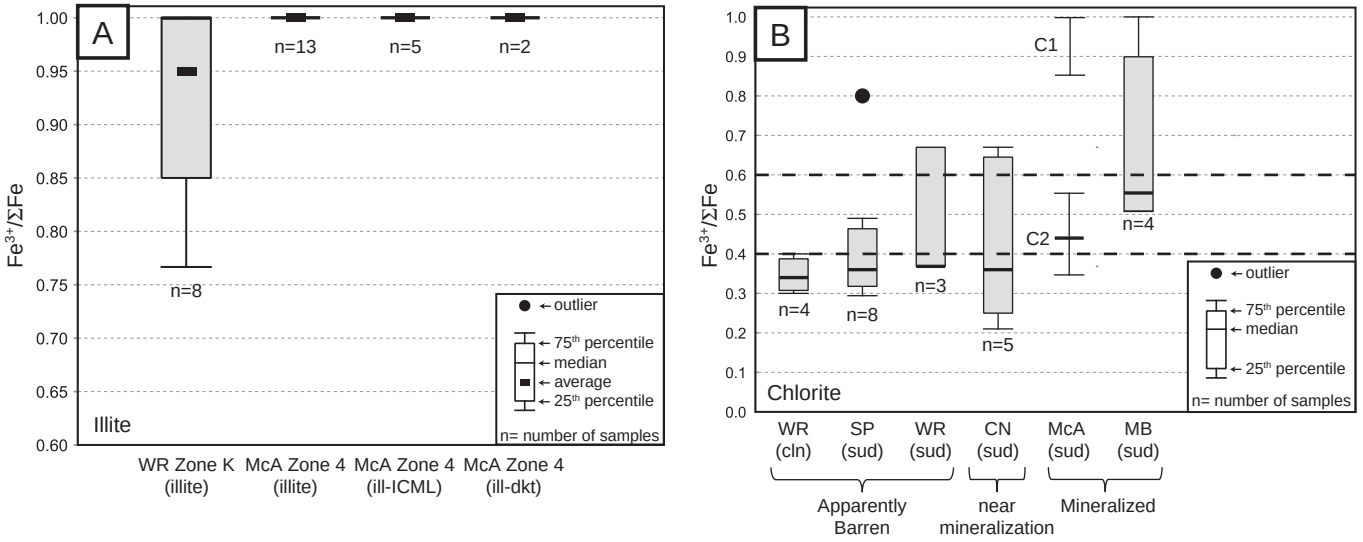

Fig. 12. Tukey boxplot comparing median $Fe^{3+}/\Sigma Fe$ ratios of illite (A) and chlorite (B) from sandstone-hosted alteration systems. Abbreviations: WR = Wheeler River, SP = Spring Point, CN = Centennial, McA = McArthur River, MB = Maurice Bay, cln = clinochlore, dkt = dickite, ill = illite, ICML = illite–chlorite mixed layer, sud = sudoite.

Fe recorded in paragenetically-constrained alteration minerals provides a record of the evolving redox conditions of the pre- and syn-ore fluids that have affected the deposits and barren areas in the basin.

Sudoite and clinochlore alteration halos in sandstone-hosted systems form around faulted unconformities, with basement rocks likely providing the source of Mg and Fe needed for its formation. The observed $Fe^{3+}/\Sigma Fe$ ratios of sudoite and clinochlore in this study support the fluid-mixing mechanism proposed for sandstone-hosted systems by Fayek and Kyser (1997) and Kotzer and Kyser (1995) wherein sudoite is produced from variable degrees of mixing between oxidizing basinal fluids and reducing basement-derived fluids (Fig. 13). Mobile Fe^{2+}, transported by reducing basement fluids, is oxidized to Fe^{3+} upon interaction with basinal fluids. Both Fe^{2+} and Fe^{3+} were subsequently incorporated into sudoite and clinochlore and Fe^{3+} into hematite. Only the partial oxidation of mobile Fe^{2+} is assumed to have occurred based on the occurrence of both structural Fe^{2+} and Fe^{3+} in the chlorite samples. The primary oxidants for Fe^{2+} were likely dissolved oxygen or U^{6+} in the basinal fluid, following the simplified redox reactions (Stumm and Morgan, 1996):

$$O_{2(aq)} + 4Fe^{2+}_{(aq)} + 4H^{+}_{(aq)} \rightarrow 4Fe^{3+}_{(sudoite,clinochlore,or\ hematite)} + 2H_2O \quad (1)$$

$$U^{6+}_{(aq)} + Fe^{2+}_{(aq)} + 2H_2O \rightarrow U^{4+}O_{2\ (uraninite)} + Fe^{3+}_{(sudoite,clinochlore,or\ hematite)} + 4H^{+}_{(aq)}. \quad (2)$$

In mechanism 2, Fe^{2+} serves one of the possible reductants of U^{6+} in the basinal fluid, thereby reducing U^{6+} to U^{4+} and causing uraninite deposition.

The occurrence of sudoite and clinochlore alteration halos with lower $Fe^{3+}/\Sigma Fe$ ratios than illite indicates that reducing basement-

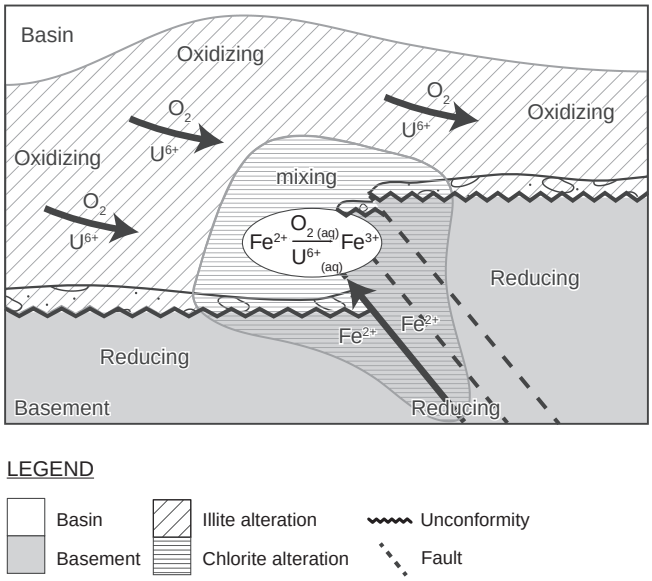

Fig. 13. Fluid-mixing model for sandstone-hosted alteration systems in the Athabasca Basin. Fe^{2+} transported by reducing basement-derived fluids emerged from basement fault structures and became oxidized to Fe^{3+} upon encountering oxidizing basinal fluids. Oxidation of Fe^{2+} occurred via a coupled redox reaction with dissolved O_2 and U^{6+}. Both Fe^{2+} and Fe^{3+} are subsequently incorporated into the chlorite alteration halo.

derived fluids were present in all five studied sandstone-hosted alteration systems (Figs. 5–9). Thus, the lack of U mineralization in the barren systems was likely not the result of reductants, such as Fe^{2+}, being absent. Results from this study indicate that sudoite samples from the alteration halos of the mineralized McArthur River Zone 4 and Maurice Bay systems were more oxidizing (median $Fe^{3+}/\Sigma Fe$ of 0.45–0.55) than sudoite and clinochlore samples from the barren alteration halos at Wheeler River Zone "K" and Spring Point and the weakly mineralized drill hole (VR-04) near Centennial (median $Fe^{3+}/\Sigma Fe$ of 0.3–0.4) (Fig. 12B). These findings are consistent with the interpretations of Alexandre et al. (2009a) and Cloutier et al. (2010) that one of the important geochemical requirements for U mineralization in sandstone-hosted deposits is the contemporaneous occurrence of flowing, oxidizing, U-bearing basinal fluids with reducing basement fluids released from basement structures. In barren systems where reducing basement-derived fluids did not interact extensively with basinal fluids to cause U deposition, Fe^{2+} was not significantly oxidized to Fe^{3+}, resulting in sudoite and clinochlore having lower $Fe^{3+}/\Sigma Fe$ ratios. In mineralized systems where continuous fluid-mixing occurred, more Fe^{2+} was oxidized to Fe^{3+}, resulting in sudoite with higher $Fe^{3+}/\Sigma Fe$ ratios.

As indicated by the $Fe^{3+}/\Sigma Fe$ ratios in sudoite and clinochlore, the redox conditions (fO_2) of pre-ore alteration fluids near the redox front differed between each system. Greater amounts of reducing basement-derived fluids contributed to sudoite and clinochlore alteration at the barren Spring Point and Wheeler River Zone "K" systems (Alexandre et al., 2009a; Cloutier et al., 2010), whereas, greater amounts of oxidizing basinal fluids contributed to the sudoite halos at the mineralized Maurice Bay and McArthur River Zone 4 deposits (Alexandre et al., 2009a). The reducing nature of the sudoite and clinochlore halos at Spring Point and Wheeler River Zone "K" is further supported by the macroscopic observation of hematite dissolution and the presence of disseminated sulfide minerals near the central portion of these alteration systems. Conditions were more oxidizing at the center of Maurice Bay (Alexandre et al., 2009a) and McArthur River Zone 4, as inferred from the strong hematite alteration associated with ore.

Sudoite from the central alteration zone at McArthur River Zone 4 is more reducing ($Fe^{3+}/\Sigma Fe = 0.34–0.56$) and contains greater Fe content (ca. 9.1 wt.% FeO_T) than sudoite from Maurice Bay ($Fe^{3+}/\Sigma Fe = 0.51–1.00$, ca. 3.5 wt.% FeO_T), suggesting that a greater concentration of mobile Fe^{2+} was available for U reduction at McArthur River. This may have contributed to the significantly higher grades and tonnages at McArthur River (ca. 332.6 Mlbs U_3O_8 at 20.69 wt.% U_3O_8; Bronkhorst et al., 2009) compared to Maurice Bay (ca. 1.5 Mlbs U_3O_8 at 0.6 wt.% U_3O_8; Mega Uranium Ltd., 2012). Furthermore, deposit-scale differences in the relative volumes of reducing and oxidizing fluids, extent of fluid-mixing, fO_2 of each fluid, host rock lithology, and the availability of other reductants, such as carbon-based compounds (e.g. CH_4) derived from the break-down of graphite, collectively contribute to the observed variations in the $Fe^{3+}/\Sigma Fe$ ratio of sudoite and clinochlore between different alteration systems.

5.2. H and Pb isotope chemistry as indicator of post-crystallization alteration of Fe oxidation state in phyllosilicates

Octahedrally-coordinated Fe cations in natural phyllosilicates are susceptible to redox changes following crystallization, including oxidation by meteoric waters (Rozenson and Heller-Kallai, 1978). Radiolysis of water in contact with U ore can also produce oxidants such as hydrogen peroxide (H_2O_2), oxygen gas (O_2), and hydroxide radicals or reductants such as hydrogen gas (H_2) or hydrogen radicals which can alter the oxidation state of structural Fe in phyllosilicates (Drago et al., 1977; Gournis et al., 2000; Liu and Neretnieks, 1996; Sattonnay et al., 2001). However, Dubessy et al. (1988) proposed that the radiolysis of water will generate an overall oxidizing fluid since oxidizing radicals and species are highly reactive whereas molecular H_2 is inert. Evidence for the post-ore radiolysis of water around Athabasca Basin unconformity-related U ore bodies is supported by molecular H_2, with and without O_2, in the vapor phase of late aqueous fluid inclusions in quartz overgrowths and veins close to the Rabbit Lake and Cluff Lake D deposits (Dubessy et al., 1988; Pagel et al., 1980) and post-ore quartz at the McArthur River deposit (Derome et al., 2005).

The mobile Pb isotopic composition of drill cores is one diagnostic indicator of the interaction between phyllosilicates with post-ore fluids. Provided that the radiogenic Pb is not supported by U in the sample, a radiogenic Pb signature would indicate that the drill core had interacted with fluids mobilizing U pathfinder elements from the deposit. This, in turn, would enable the redox products of water radiolysis forming near the deposit to be transported to the surrounding alteration halo. Alternatively, post-crystallization fluid interaction can also be indicated by the hydrogen isotopic composition of the phyllosilicates, as hydrogen in hydroxyl groups is highly susceptible to isotopic exchange. Hydrogen isotopic exchange with low-temperature (<50 °C), low δD, post-Cretaceous (ca. −110‰; Halter et al., 1987) to modern-day (ca. −150‰; Kotzer and Kyser, 1995; Wilson and Kyser, 1987) meteoric waters, with or without radiation-induced catalysis, has been invoked for causing ^2H-depletion in illite and chlorite around several Athabasca Basin U deposits. Alternatively, Bray et al. (1988) proposed that low δD fluid values associated with the hydrothermal alteration halo around the McClean Lake U deposit resulted from basinal fluids interacting with $CH_4 \pm H_2S \pm H_2$ contained in graphitic metasedimentary basement rocks. Interaction with H_2 produced from water radiolysis would also cause ^2H-depletion in clays as radiolytic H_2 has δD values of approximately −500‰ (Lin et al., 2005). As recent meteoric waters of the Athabasca Basin and the redox products generated by water radiolysis are ^2H-depleted species, in-situ oxidation or reduction of structural Fe caused by interaction with these redox agents will be reflected in a correlation between the $Fe^{3+}/\Sigma Fe$ ratios and δD values of the phyllosilicates.

No correlation is observed between the $Fe^{3+}/\Sigma Fe$ and δD values for illite from Wheeler River Zone "K" and McArthur River Zone 4 indicating that the $Fe^{3+}/\Sigma Fe$ ratios recorded by these alteration minerals were only minimally affected by post-crystallization fluids (Fig. 14A). At McArthur River Zone 4, where the ore body could have potentially caused water radiolysis, drill cores containing illite record non-radiogenic Pb isotope signatures suggesting a lack of interaction with post-ore fluids interacting with the Zone 4 mineralization (Fig. 14A; Table 3). Furthermore, illite samples from both McArthur River Zone 4 and Wheeler River Zone "K" have δD values above −70‰ suggesting that it had not undergone significant hydrogen isotope exchange with relatively recent ^2H-depleted meteoric waters (Table 2). These δD mineral values are greater than those of illite and chlorite from the mineralized zone at the Cluff Lake U deposit (δD = −90 to −170‰) which experienced radiation-catalyzed hydrogen isotopic exchange with meteoric water (Halter et al., 1987). Both the hydrogen and Pb isotope results provide support that the $Fe^{3+}/\Sigma Fe$ ratios recorded by these illite likely remained unchanged after crystallization.

Sudoite and clinochlore samples from the studied alteration systems have radiogenic Pb isotope ratios, with the most radiogenic Pb ratios observed in sudoite-bearing drill cores near the unconformities at McArthur River Zone 4, Maurice Bay, and Centennial VR-04, likely mobilized from nearby high-grade U mineralization at these locations (Table 3). The $Fe^{3+}/\Sigma Fe$ ratios of both sudoite and clinochlore from McArthur River Zone 4, Maurice Bay, Wheeler River Zone "K", and Spring Point are non-correlated with their δD values suggesting that neither interaction with post-ore fluids from the deposit or meteoric waters caused changes to the oxidation state of structural Fe (Fig. 14B). The only exception is the sudoite samples from Centennial VR-04, in which the $Fe^{3+}/\Sigma Fe$ ratios are weakly correlated with δD values (Figs. 7, 14B). The two sudoite separates near the unconformity at VR-04

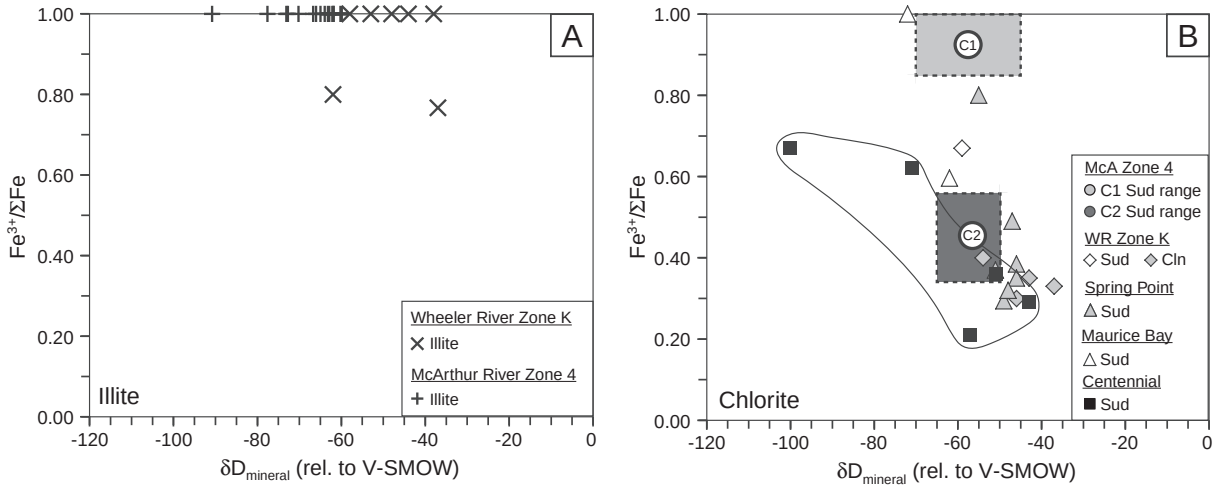

Fig. 14. Relationship between $Fe^{3+}/\Sigma Fe$ ratio and δD value for illite (A) and chlorite (B) from studied sandstone-hosted alteration systems. See in-text for discussion.

(Centennial) that are most depleted in ^{2}H (δD = −71 and −100‰) also have the highest $Fe^{3+}/\Sigma Fe$ ratios, suggesting that the chemical process responsible for ^{2}H-depletion coincided with the oxidation of structural Fe^{2+} within these sudoite samples (Fig. 7). As both sudoite samples occur near the permeable unconformity, interaction with relatively recent meteoric waters or the oxidants produced by radiolysis mobilized from the nearby Centennial ore body are two possible mechanisms causing oxidation (Fig. 7). However, the near-origin U–Pb lower intercept ages of uraninite and high abundance of late uranophane in veins (ca. 2 Ma) at the nearby Centennial deposit supports the interpretation involving the incursion of recent low δD meteoric fluids (Alexandre et al., 2012).

5.3. Evolution of the oxidation state of Fe and its relationship with the genesis of sandstone-hosted alteration systems

The genetic evolution of sandstone-hosted alteration systems consists of four main alteration stages, each characterized by the formation of a dominant Fe-bearing mineral: early, mid, and late pre-ore alteration, and ore stages (Fig. 3). Early pre-ore alteration in sandstone-hosted systems produced hematite in the Athabasca Group sandstones (Stage 1, Fig. 3). The presence of hematite and goyazite and the paucity of detrital pyrite indicate that early diagenetic basinal fluids within the Athabasca Group were oxidizing, with Fe and S liberated from pyrite oxidized entirely to Fe^{3+} and sulfate. Fluids of high fO_2 would have enabled the transport of high concentrations of dissolved U leached from detrital minerals (e.g. Fayek and Kyser, 1997; Komninou and Sverjensky, 1996).

Mid pre-ore alteration is characterized by phyllosilicate-dominated alteration of the Athabasca Group from a basinal fluid that remained relatively oxidizing (Stage 2, Fig. 3). In the Read and Manitou Falls Formations at Wheeler River Zone "K", this produced illite alteration having $Fe^{3+}/\Sigma Fe$ ratios between 0.77 and 1.00 (Fig. 6). At McArthur River Zone 4, mid pre-ore alteration produced early-stage C1 sudoite, with $Fe^{3+}/\Sigma Fe$ ratios between 0.85 and 1.00, and later-formed illite and ICML clay containing only Fe^{3+} (Fig. 5). The presence of minor Fe^{2+} in these phyllosilicate minerals suggests the addition of Fe^{2+} prior to crystallization. At Wheeler River Zone "K", the addition of Fe^{2+} was likely from fluids originating from the underlying basement as supported by the enrichment in ^{2}H of illite, which may reflect a greater contribution of basement fluids (Fig. 10; Cloutier et al., 2010). In general, basement-derived fluids associated with sandstone-hosted deposits have higher δD values (ca. −30‰) compared to basinal fluids (ca. −60‰) (Kotzer and Kyser, 1995). At McArthur River Zone 4, however, the source of Fe^{2+} in early C1 sudoite was likely not derived from the basement since a 200 m-thick early pre-ore silicified zone overlying the unconformity would have prevented reducing basement-derived fluids from reaching above MFb (Fig. 5). Furthermore, neither illite nor ICML clay occurring stratigraphically below and paragenetically after C1 sudoite contains Fe^{2+} (Fig. 5). Thus, the likeliest source of Fe^{2+} for early C1 Mg-sudoite was from the original sediments in this stratigraphic unit that underwent closed-system diagenesis. The slightly higher and more restricted range of δD values for the fluid in equilibrium with Wheeler River Zone "K" illite compared to McArthur River Zone 4 illite is interpreted as reflecting greater contributions of a basement-derived fluid in the former and a predominantly basinal fluid signature in the latter. Calculated formation temperatures of mid pre-ore illite indicate fluid temperatures of ca. 180–240 °C, although the majority formed within a restricted range between 220 and 240 °C (Table 1). These temperatures are consistent with those generally proposed for peak diagenesis in the Athabasca Basin (ca. 200 °C; Hoeve and Sibbald, 1978).

Late pre-ore sudoite and clinochlore alteration formed halos around faulted unconformities in each sandstone-hosted alteration system (Stage 3, Figs. 3, 5–9). The spatial association between these chlorite halos with the faulted unconformity and the generally lower $Fe^{3+}/\Sigma Fe$ ratios of sudoite and clinochlore compared to illite (Fig. 12B), suggest that reducing basement-derived fluids contributed to chlorite alteration. This is supported by the greater δD values of the fluid forming hydrothermal C2 sudoite compared to diagenetic C1 sudoite at McArthur River Zone 4, indicating the former had a greater basement contribution, in agreement with its closer proximity to the faulted unconformity. Calculated formation temperatures for late hydrothermal sudoite from the studied alteration systems indicate fluid temperatures of ca. 150–200 °C which are slightly lower than peak diagenetic temperatures recorded by illite (ca. 180–240 °C; Table 1). Calculated formation temperature for clinochlore which postdates sudoite at Wheeler River Zone "K" is ca. 230 °C, closely similar to that of peak-diagenetic illite. The lower formation temperatures of sudoite compared to illite likely reflect the inaccuracy of the chlorite geothermometer for sudoite rather than signifying cooling of fluid temperatures during hydrothermal alteration. Uncertainties in the sudoite formation temperatures arise because the chlorite geothermometers were calibrated using trioctahedral chlorite and the fine grain size of sudoite makes their analysis by electron microprobe difficult. Zang and Fyfe (1995) also noted that corrections for $^{[4]}Al$ occupancy based on Fe/Fe + Mg ratios may lead to large corrections to $^{[4]}Al$ which would yield lower calculated temperatures. Thus, the calculated temperatures for chlorite should be considered as their minimum formation temperatures. Factoring in the large error

margins of ±25 °C, the formation temperatures of hydrothermal sudoite are near 200 °C and similar to peak diagenetic temperatures. The timing of sudoite and clinochlore alteration is bracketed by the timing of pre-ore illite alteration (ca. 1675 Ma) and the main U mineralization event (ca. 1590 Ma, Alexandre et al., 2009b). Mixing of reducing basement-derived fluids with oxidizing basinal fluids would have significantly changed the fluid chemistry of the basinal fluid, in particular, decreasing its fO_2 (Komninou and Sverjensky, 1996). Depending on the degree of mixing between these two contrasting fluids, this would affect the relative proportion of Fe^{2+} and Fe^{3+}, producing the observed differences in $Fe^{3+}/\Sigma Fe$ ratios of sudoite and clinochlore samples between the studied systems. The spatially-extensive, relatively reduced sudoite and clinochlore halos at Wheeler River Zone "K" and Spring Point suggest that reducing basement-derived fluids were involved in creating these alteration systems but insufficient U-bearing oxidizing basinal fluids were present to form a deposit (Figs. 6, 9). This differs from the more oxidizing alteration conditions attained in the mineralized Maurice Bay and McArthur River Zone 4 systems, as suggested by their illite-dominated alteration assemblages and more oxidized sudoite alteration halos (Figs. 5, 8).

U mineralization was initiated at ca. 1590 Ma (Alexandre et al., 2009b), following or nearly synchronous with sudoite alteration near the faulted unconformity (Stage 4, Fig. 3). The presence of strong hematite alteration associated with uraninite at McArthur River Zone 4, Maurice Bay, and Centennial suggests coupled redox reaction between mobile Fe^{2+} in the basement fluid and U^{6+} in the basinal fluid to form Fe^{3+}, which precipitated as hematite and U^{4+} as uraninite (Alexandre et al., 2012; McGill et al., 1993). Such a discrepancy between the slightly earlier paragenetic timing of sudoite relative to U mineralization may be a result of sudoite being stable under a larger range of fO_2 conditions (Kister et al., 2005), whereas, U deposition occurs only under reducing conditions. Thus, sudoite may have been able to form under more oxidizing fluid conditions during the initial stages of fluid mixing, whereas uraninite would have precipitated later when the fO_2 of the mineralized fluid decreased and the redox front became more reducing as more basement fluids were added.

5.4. Significance of $Fe^{3+}/\Sigma Fe$ ratios as an exploration tool

The spatial variation in the $Fe^{3+}/\Sigma Fe$ ratio of sudoite may be used as a geochemical vector to the source of reducing fluid. Trends of decreasing $Fe^{3+}/\Sigma Fe$ ratios in sudoite, when coupled with decreasing $^{207}Pb/^{206}Pb$ ratios of leachable Pb from drill core, can be a reliable geochemical vector towards sandstone-hosted unconformity-related U deposits (Fig. 15; Table 3). The $Fe^{3+}/\Sigma Fe$ ratio of sudoite and $^{207}Pb/^{206}Pb$ ratio of leachable Pb both broadly decrease with increasing proximity to the faulted unconformities at McArthur River Zone 4 (C2 sudoite) and Maurice Bay (Fig. 15A, C). This is in agreement with the fault structure in these alteration systems being the conduit for reducing, Fe^{2+}-bearing basement-derived fluids and the ore bodies being the source of radiogenic Pb that were mobilized by post-ore fluids circulating into the reactivated fault (Figs. 5, 8). At Wheeler River Zone "K", clinochlore samples show non-varying $Fe^{3+}/\Sigma Fe$ ratios with respect to distance from the Zone "K" shear zone (Fig. 15B). $Fe^{3+}/\Sigma Fe$ ratios of sudoite broadly decrease towards the shear zone but are not correlated with increasing radiogenic Pb signatures (decreasing $^{207}Pb/^{206}Pb$), in agreement with the lack of sandstone-hosted U mineralization at Zone "K" (Figs. 6, 15B). The lack of systematic spatial variation in the $^{207}Pb/^{206}Pb$ ratios in Wheeler River Zone "K" drill cores suggests that radiogenic Pb was unlikely to have been remobilized from a common radiogenic source, such as the weakly mineralized basement (0.17% U_3O_8 over 7.7 m; Gamelin et al., 2010).

In the Spring Point alteration system, neither the $^{207}Pb/^{206}Pb$ of leachable Pb nor the $Fe^{3+}/\Sigma Fe$ ratios in sudoite show systematic spatial variations with respect to the Spring Bay Fault (Fig. 15D). In fact, both parameters remain relatively uniform up to ca. 900 m from the fault zone. The consistent $^{207}Pb/^{206}Pb$ ratios are in agreement with U mineralization being absent at Spring Point, whereas, the constant $Fe^{3+}/\Sigma Fe$ ratios indicate homogeneous redox conditions within the sudoite alteration halo. This indicates that reducing basement-derived fluids had limited interaction with oxidizing fluids during hydrothermal alteration at Spring Point.

Sudoite samples from drill hole VR-04, distal to the Centennial deposit, show a trend of increasing $Fe^{3+}/\Sigma Fe$ ratios towards the weakly-mineralized unconformity (Figs. 7; 15E). Such a trend is atypical for sandstone-hosted systems where the basement represents the source of the reducing fluids. As indicated by δD mineral values, in-situ oxidation of Fe^{2+} by meteoric waters has affected the oxidation state of Fe in sudoite samples near the unconformity (Figs. 7, 14B). The remaining sudoite samples, which were unaffected by post-crystallization redox changes, have $Fe^{3+}/\Sigma Fe$ ratios similar to barren systems. This is in agreement with the absence of interaction with U-bearing basinal fluids and the lack of U mineralization in VR-04 (Table 3). The decreasing $^{207}Pb/^{206}Pb$ ratio towards the unconformity is likely the result of radiogenic Pb migrating from the Centennial ore body along the permeable unconformity surface (Alexandre et al., 2012).

Broad trends of decreasing $Fe^{3+}/\Sigma Fe$ ratios in sudoite samples with proximity to the faulted unconformities are observed for both barren and mineralized systems (Fig. 15A–C). This indicates that $Fe^{3+}/\Sigma Fe$ ratios recorded by sudoite, unlike the leachable $^{207}Pb/^{206}Pb$ ratios from drill cores, are not a vector to U mineralization but reflect the proximity to the source of reducing fluids.

6. Summary

Sandstone-hosted unconformity-related U deposits in the Athabasca Basin are surrounded by spatially-extensive pre-ore clay alteration halos characterized by an outer, peripheral zone of illite alteration and overprinted by an inner, proximal zone of chlorite alteration. Illite in the Athabasca Group precipitated primarily from an oxidizing basinal fluid, whereas, hydrothermal sudoite and clinochlore formed near sites where the basal Athabasca Group were disrupted by fault structures rooted in the basement and from reducing basement-derived fluids that experienced varying degrees of mixing with oxidizing basinal fluids. This resulted in the oxidation of mobile Fe^{2+}, transported by the reducing fluid, to Fe^{3+}, with both oxidation states of Fe subsequently being incorporated into sudoite and clinochlore and Fe^{3+} into hematite. Higher $Fe^{3+}/\Sigma Fe$ ratios are recorded in sudoite from the center of mineralized systems at McArthur River Zone 4 and Maurice Bay than in sudoite and clinochlore from apparently barren systems at Wheeler River Zone "K" and Spring Point. Therefore, the critical geochemical factor which precluded U mineralization in barren systems is the lack of U-bearing oxidizing basinal fluids available for mixing with reducing basement-derived fluids emerging from basement conduits. Broad trends of decreasing $Fe^{3+}/\Sigma Fe$ ratios in sudoite with distance to fault zones, in both mineralized and non-mineralized systems, suggest that the spatial variation in $Fe^{3+}/\Sigma Fe$ ratios of sudoite reflects their proximity to the source of reducing fluid rather than to U mineralization, with sudoite in the distal portions of the alteration halos being more oxidized (higher $Fe^{3+}/\Sigma Fe$).

Apparently barren alteration systems at Wheeler River Zone "K" and Spring Point are associated with large halos of sudoite and clinochlore alteration with low $Fe^{3+}/\Sigma Fe$ ratios indicating a reducing alteration system that did not encounter significant volumes of oxidizing basinal fluids. In contrast, sandstone-hosted alteration systems near mineralized deposits at McArthur River Zone 4 and Maurice Bay have illite-dominated alteration assemblages and small halos of sudoite alteration with higher $Fe^{3+}/\Sigma Fe$ ratios, reflecting greater contribution of oxidizing basinal fluids transporting U from the basin.

Finally, the $Fe^{3+}/\Sigma Fe$ ratio recorded by sudoite and clinochlore can be used as an indirect monitor of the degree of mixing between oxidizing and reducing fluids, allowing alteration systems to be

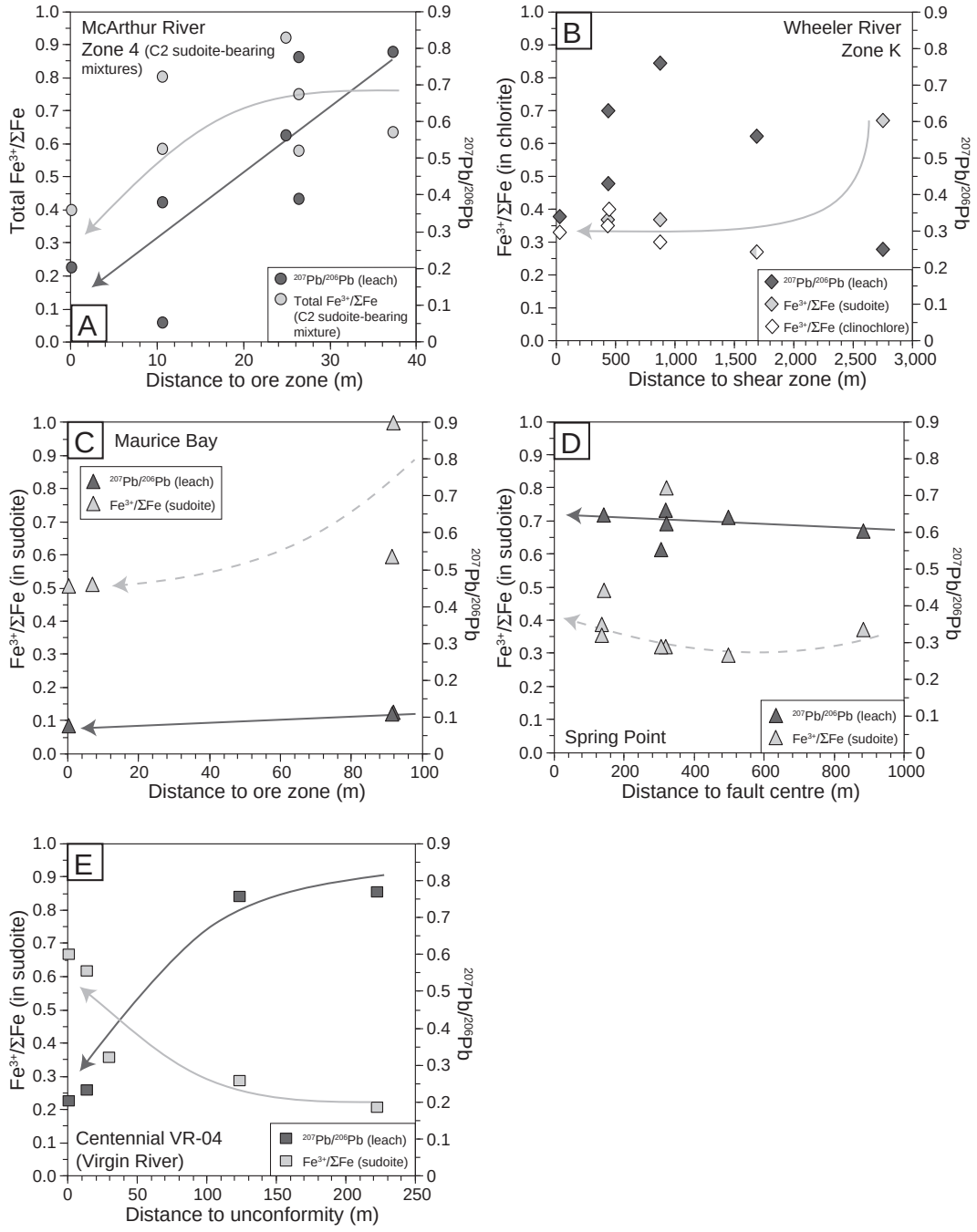

Fig. 15. Relationship between $^{207}Pb/^{206}Pb$ ratio of leachable Pb and $Fe^{3+}/\Sigma Fe$ ratio of chlorite with distance to major basement structures and ore bodies. A. McArthur River Zone 4 C2 sudoite-bearing mixtures. B. Wheeler River Zone "K" sudoite and clinochlore. C. Maurice Bay sudoite. D. Spring Point sudoite. E. Sudoite from drill hole VR-04 near the Centennial deposit. See in-text for discussion.

evaluated for their potential to contain sandstone-hosted unconformity-related U deposits. Trends of decreasing $Fe^{3+}/\Sigma Fe$ ratio in sudoite when correlated with decreasing $^{207}Pb/^{206}Pb$ ratios of leachable Pb can be a spatial vector to U mineralization.

Acknowledgments

This work benefited from a NSERC Collaborative Research and Discovery grant and financial and field support from Cameco Corporation. Special thanks are made to Brian Joy at Queen's University for assistance with electron microprobe measurements. Dan Jiricka and Gary Witt from Cameco Corporation are thanked for providing logistical support in the field. Revisions by Don Chipley and Steve Beyer were helpful in improving this manuscript. We wish to also thank the two anonymous reviewers for their constructive comments on this manuscript. Kreeti Saravanan and Prof. Benedetto De Vivo are thanked for editorial handling.

References

Alexandre, P., Kyser, K., Polito, P., Thomas, D., 2005. Alteration mineralogy and stable isotope geochemistry of Paleoproterozoic basement-hosted unconformity-type uranium deposits in the Athabasca Basin, Canada. Economic Geology 100, 1547–1563.

Alexandre, P., Kyser, K., Jiricka, D., 2009a. Critical geochemical and mineralogical factors for the formation of unconformity-related uranium deposits: comparison between

barren and mineralized systems in the Athabasca Basin, Canada. Economic Geology 104, 413–435.
Alexandre, P., Kyser, K., Thomas, D., Polito, P., Marlat, J., 2009b. Geochronology of unconformity-related uranium deposits in the Athabasca Basin, Saskatchewan, Canada and their integration in the evolution of the basin. Mineralium Deposita 44, 41–59.
Alexandre, P., Kyser, K., Jiricka, D., Witt, G., 2012. Formation and evolution of the Centennial unconformity-related uranium deposit in the south-central Athabasca Basin, Canada. Economic Geology 107, 385–400.
Annesley, I.R., Madore, C., Portella, P., 2005. Geology and thermotectonic evolution of the western margin of the Trans-Hudson Orogen: evidence from the eastern sub-Athabasca basement, Saskatchewan. Canadian Journal of Earth Sciences 42, 573–597.
Arseneau, G., Revering, C., 2010. Technical report on the Phoenix deposit (Zones A and B)-Wheeler River project, eastern Athabasca Basin, Northern Saskatchewan, Canada. Denison Mines Corporation, NI 43-101 Technical Report. (96 pp.).
Bailey, S.W., Lister, J.S., 1989. Structures, compositions, and X-ray identification of dioctahedral chlorites. Clays and Clay Minerals 37, 193–202.
Berman, R.G., Bostock, H.H., 1997. Metamorphism in the northern Taltston magmatic zone, Northwest Territories. The Canadian Mineralogist 35, 1069–1091.
Berman, R.G., Davis, W.J., Pehrsson, S., 2007. Collisional Snowbird tectonic zone resurrected: growth of Laurentia during the 1.9 Ga accretionary phase of the Hudsonian orogeny. Geology 35, 911–914.
Billault, V., Beaufort, D., Patrier, P., Petit, S., 2002. Crystal chemistry of Fe-sudoites from uranium deposits in the Athabasca Basin (Saskatchewan, Canada). Clays and Clay Minerals 50, 70–81.
Bray, C.J., Spooner, E.T.C., Longstaffe, F.J., 1988. Unconformity-related uranium mineralization, McClean deposits, northern Saskatchewan, Canada: hydrogen and oxygen isotope geochemistry. The Canadian Mineralogist 26, 249–268.
Bronkhorst, D., Edwards, C.R., Mainville, A.G., Murdock, G.M., Yesnik, L.D., 2009. McArthur River operation, Northern Saskatchewan, Canada. Cameco Corporation, NI 43-101 Technical Report. (207 pp.).
Card, C.D., 2001. Basement rocks to the western Athabasca Basin in Saskatchewan. Saskatchewan Geological Survey, Saskatchewan Energy and Mines, Miscellaneous Report 2001-4-2: Summary of Investigations 2001, vol. 2, pp. 321–333.
Cathelineau, M., 1988. Cation site occupancy in chlorites and illites as a function of temperature. Clay Minerals 23, 471–485.
Clayton, R.N., Mayeda, T.K., 1963. The use of bromine pentafluoride in the extraction of oxygen from oxides and silicates for isotopic analysis. Geochimica et Cosmochimica Acta 27, 43–52.
Cloutier, J., Kyser, K., Olivo, G.R., Alexandre, P., Halaburda, J., 2009. The Millenium uranium deposit, Athabasca Basin, Saskatchewan, Canada: an atypical basement-hosted unconformity-related uranium deposit. Economic Geology 104, 815–840.
Cloutier, J., Kyser, K., Olivo, G.R., Alexandre, P., 2010. Contrasting patterns of alteration at the Wheeler River area, Athabasca Basin, Saskatchewan, Canada: insights into the apparently uranium-barren Zone K alteration system. Economic Geology 105, 303–324.
Cloutier, J., Kyser, K., Olivo, G.R., 2011. Geochemical, isotopic, and geochronlologic constraints on the formation of the Eagle Point basement-hosted uranium deposit, Athabasca Basin, Saskatchewan, Canada and recent remobilization of primary uraninite in secondary structures. Mineralium Deposita 46, 35–56.
Cumming, G.L., Krstic, D., 1992. The age of unconformity-related uranium mineralization in the Athabasca Basin, northern Saskatchewan. Canadian Journal of Earth Sciences 29, 1623–1639.
Derome, D., Cathelineau, M., Cuney, M., Cecil, F., Lhomme, T., 2005. Mixing of sodic and calcic brines and uranium deposition at McArthur River, Saskatchewan, Canada: a Raman and laser-induced breakdown spectroscopic study of fluid inclusions. Economic Geology 100, 1529–1545.
Drago, V., Baggio Saittovich, E., Danon, J., 1977. Mössbauer spectroscopy of electron irradiated natural layered silicates. Journal of Inorganic and Nuclear Chemistry 39, 973–979.
Dubessy, J., Pagel, M., Beny, J.M., Christensen, H., Nickel, B., Kosztolanyi, C., Poty, B., 1988. Radiolysis evidenced by H_2–O_2 and H_2-bearing fluid inclusions in three uranium deposits. Geochimica et Cosmochimica Acta 52, 1155–1167.
Eslinger, E.V., Savin, S.M., 1973. Mineralogy and oxygen isotope geochemistry of the hydrothermally altered rocks of the Ohaki-Broadlands, New Zealand, geothermal area. American Journal of Science 273, 240–267.
Fanning, D.S., Rabenhorst, M.C., May, L., Wagner, D.P., 1989. Oxidation state of iron in glauconite from oxidized and reduced zones of soil-geologic columns. Clays and Clay Minerals 37, 59–64.
Fayek, M., Kyser, T.K., 1997. Characterization of multiple fluid-flow events and rare-earth-element mobility associated with formation of unconformity-type uranium deposits in the Athabasca Basin, Saskatchewan. The Canadian Mineralogist 35, 627–658.
Fayek, M., Kyser, T.K., Riciputi, L.R., 2002. U and Pb isotope analysis of uranium minerals by ion microprobe and the geochronology of the McArthur River and Sue Zone uranium deposits, Saskatchewan, Canada. The Canadian Mineralogist 40, 1553–1569.
Gamelin, C., Sorba, D., Kerr, W., 2010. The discovery of the Phoenix deposit: a new high-grade Athabasca Basin unconformity-type uranium deposit, Saskatchewan, Canada. Saskatchewan Geological Open House 2010 Conference, Saskatoon, Nov 29–Dec 1, 2010 (technical session talk online at http://economy.gov.sk.ca/Default.aspx?DN=b14d0dda-3019-4238-b55b-413cb5328583).
Gournis, D., Mantaka-Marketou, A.E., Karakassides, M.A., Petridis, D., 2000. Effect of γ-irradiation of clays and organoclays: a Mössbauer and XRD study. Physics and Chemistry of Minerals 27, 512–521.
Halter, G., Sheppard, S.M.F., Weber, F., Clauer, N., Pagel, M., 1987. Radiation-related retrograde hydrogen isotope and K–Ar exchange in clay minerals. Nature 330, 638–641.
Hanmer, S., Sandeman, H.A., Davis, W.J., Aspler, L.B., Rainbird, R.H., Ryan, J.J., Relf, C., Peter, T.D., 2004. Geology and Neoarchean tectonic setting of the central Hearne supracrustal belt, Western Churchill Province, Nunavut, Canada. Precambrian Research 134, 63–83.
Harper, C.T., 1996. Geology of the Maurice Bay area (NTS 74N-5 and part of 74N-12). In: Sibbald, T.I.I. (Ed.), Saskatchewan Geological Survey, Saskatchewan Energy and Mines, Report 219 (27 pp.).
Hiatt, E.E., Kyser, T.K., Fayek, M., Polito, P., Holk, G.J., Riciputi, L.R., 2007. Early quartz cements and evolution of paleohydraulic properties of basal sandstones in three Paleoproterozoic continental basins: evidence from in situ $\delta^{18}O$ analysis of quartz cements. Chemical Geology 238, 19–37.
Hinckley, D.N., 1963. Variability in "crystallinity" values among the kaolin deposits of the coastal plain of Georgia and South Carolina. Clay and Clay Minerals 11, 229–235.
Hoeve, J., Sibbald, T.I.I., 1978. On the genesis of Rabbit Lake and other unconformity-type uranium deposits in northern Saskatchewan, Canada. Economic Geology 73, 1450–1473.
Hoffman, P.F., 1988. United plates of America, the birth of a craton: early Proterozoic assembly and growth of Laurentia. Annual Review of Earth and Planetary Sciences 16, 543–603.
Hoffman, P.F., 1989. Precambrian geology and tectonic history of North America. In: Bally, A.W., Palmer, A.R. (Eds.), The Geology of North America—an Overview: Geological Society of America, vol. A, pp. 447–512.
Holk, G.J., Kyser, T.K., Chipley, D., Hiatt, E.E., Marlatt, J., 2003. Mobile Pb-isotopes in Proterozoic sedimentary basins as guides for exploration of uranium deposits. Journal of Geochemical Exploration 80, 297–320.
Jefferson, C.W., Thomas, D.J., Gandhi, S.S., Ramaekers, P., Delaney, G., Brisbin, D., Cutts, C., Quirt, D., Portella, P., Olson, R.A., 2007. Unconformity-associated uranium deposits of the Athabasca Basin, Saskatchewan and Alberta. In: Jefferson, C.W., Delaney, G. (Eds.), EXTECH IV: Geology and Uranium EXploration TECHnology of the Proterozoic Athabasca Basin, Saskatchewan and Alberta: Geological Survey of Canada, Bulletin, 588, pp. 23–67.
Jiricka, D.E., Witt, G., 2008. The Centennial deposit—an atypical unconformity-associated uranium deposit. Mining Forum, Calgary, April 2008.
Kerr, W.C., 2010. The discovery of the Phoenix deposit: a new high-grade, Athabasca Basin unconformity-type uranium deposit, Saskatchewan, Canada. In: Goldfarb, R.J., Marsh, E.E., Monecke, T. (Eds.), The Challenge of Finding New Mineral Resources: Global Metallogeny, Innovative Exploration, and New Discoveries: Society of Economic Geologists, Special Publication, Vol. 2 (15): Zinc–Lead, Nickel–Copper–PGE, and Uranium, pp. 703–728.
Kister, P., Vieillard, P., Cuney, M., Quirt, D., Laverret, E., 2005. Thermodynamic constraints on the mineralogical and fluid composition evolution in a clastic sedimentary basin: the Athabasca Basin (Saskatchewan, Canada). European Journal of Mineralogy 17, 325–342.
Komninou, A., Sverjensky, D.A., 1996. Geochemical modeling of the formation of an unconformity-type uranium deposit. Economic Geology 91, 590–606.
Kotzer, T.G., Kyser, T.K., 1995. Petrogenesis of the Proterozoic Athabasca Basin, northern Saskatchewan, Canada, and its relation to diagenesis, hydrothermal uranium mineralization and Paleohydrogeology. Chemical Geology 120, 45–89.
Kyser, K., Cuney, M., 2008. Geochemical characteristics of uranium and analytical methodologies. In: Cuney, M., Kyser, K. (Eds.), Recent and Not-so-recent Developments in Uranium Deposits and Implications for Exploration: Mineralogical Association of Canada, Short Course, vol. 39, pp. 23–56.
LeCheminant, A.N., Heaman, L.M., 1989. Mackenzie igneous events, Canada: Middle Proterozoic hotspot magmatism associated with ocean opening. Earth and Planetary Science Letters 96, 38–48.
Lewry, J.F., Sibbald, T.I.I., 1980. Thermotectonic evolution of the Churchill province in northern Saskatchewan. Tectonophysics 68, 45–82.
Lin, L.H., Slater, G.F., Lollar, B.S., Lacrampe-Coulome, G., Onstott, T.C., 2005. The yield and isotopic composition of radiolytic H_2, a potential source for the deep subsurface biosphere. Geochimica et Cosmochimica Acta 69, 893–903.
Liu, J., Neretnieks, I., 1996. A model for radiation energy deposition in natural uranium-bearing systems and its consequences to water radiolysis. Journal of Nuclear Materials 231, 103–112.
Marumo, K., Nagasawa, K., Kuroda, Y., 1980. Mineralogy and hydrogen isotope geochemistry of clay minerals in the Ohnuma geothermal area, northeastern Japan. Earth and Planetary Science Letters 47, 255–262.
McGill, B.D., Marlatt, J.L., Matthews, R.B., Sopuk, V.J., Homeniuk, L.A., Hubregtse, J.J., 1993. The P2 North uranium deposit, Saskatchewan, Canada. Exploration and Mining Geology 2, 321–331.
Mega Uranium Ltd., 2012. Mega commences drill program on northwest Athabasca property. Mega Uranium Mining & Exploration in Australia: News Room. (Published January 23, 2012, last accessed January 15, 2013, article online at http://www.megauranium.com/news_room/2012/index.php?&content_id=391).
Mercadier, J., Richard, A., Cuney, M., 2012. Boron- and magnesium-rich marine brines at the origin of giant unconformity-related uranium deposits: δ11B evidence from Mg-tourmalines. Geology 40, 231–234.
Murad, E., Wagner, U., 1994. The Mössbauer spectrum of illite. Clay Minerals 29, 1–10.
Mwenifumbo, C.J., Elliott, B.E., Jefferson, C.W., Bernius, G.R., Pflug, K.A., 2004. Physical rock properties from the Athabasca Group: designing geophysical exploration models for unconformity uranium deposits. Journal of Applied Geophysics 55, 117–135.
Pagel, M., Poty, B., Sheppard, S.M.F., 1980. Contributions to some Saskatchewan uranium deposits mainly from fluid inclusions and isotopic data. In: Ferguson, S., Goleby, A. (Eds.), Uranium in the Pine Creek Geosyncline. International Atomic Energy Agency, Vienna, pp. 639–654.
Percival, J.B., Kodama, H., 1989. Sudoite from Cigar Lake, Saskatchewan. The Canadian Mineralogist 27, 633–641.
Percival, J.B., Bell, K., Torrance, J.K., 1993. Clay mineralogy and isotope geochemistry of the alteration halo at Cigar Lake uranium deposit. Canadian Journal of Earth Sciences 30, 689–704.

Quirt, D.H., 1985. Lithogeochemistry of the Athabasca Group: summary of sandstone data. Summary of Investigations 1985, Saskatchewan Geological Survey, Saskatchewan Energy and Mines, Miscellaneous Report 85-4, pp. 128–132.
Quirt, D.H., 1986. Host rock alteration in the Spring Point Area, northern Saskatchewan. Saskatchewan Research Council, Publication R-855-9-C-86. (66 pp.).
Ramaekers, P., 1990. Geology of the Athabasca Group (Helikian) in northern Saskatchewan. In: Harper, C.T., Richmond-Johnson, N. (Eds.), Saskatchewan Geological Survey, Saskatchewan Energy and Mines, Report 195 (49 pp.).
Ramaekers, P., Yeo, G., Jefferson, C., 2001. Preliminary overview of regional stratigraphy in the late Paleoproterozoic Athabasca Basin, Saskatchewan and Alberta. Saskatchewan Geological Survey, Saskatchewan Energy and Mines, Miscellaneous Report 2001–4.2: Summary of Investigations 2001, vol. 2, pp. 240–251.
Ramaekers, P., Jefferson, C.W., Yeo, G.M., Collier, B., Long, D.G.F., Drever, G., McHardy, S., Jiricka, D., Cutts, C., Wheatley, K., Catuneanu, O., Bernier, S., Kupsch, B., Post, R.T., 2007. Revised geological map and stratigraphy of the Athabasca Group, Saskatchewan and Alberta. In: Jefferson, C.W., Delaney, G. (Eds.), EXTECH IV: Geology and Uranium EXploration TECHnology of the Proterozoic Athabasca Basin, Saskatchewan and Alberta: Geological Survey of Canada, Bulletin, 588, pp. 155–191.
Rancourt, D.G., Ping, J.Y., 1991. Voigt-based methods for arbitrary-shape static hyperfine parameter distributions in Mössbauer spectroscopy. Nuclear Instruments and Methods in Physics Research B58, 85–97.
Reid, K.D., Ansdell, K., Jiricka, D., Witt, G., Card, C., 2010. Regional setting and general characteristics of the Centennial unconformity-related uranium deposit. Athabasca Basin, Saskatchewan: GeoCanada 2010 Conference, Calgary, May 10–14, 2010 (abstract online at http://www.cspg.org/documents/Conventions/Archives/Annual/2010/0838_GC2010_Regional_Setting_of_Centennial_Unconformity-related_Uranium_Deposit.pdf).
Reid, K.D., Ansdell, K., Jiricka, D., Witt, G., 2011. Composition and timing of chlorites at the Centennial unconformity-related uranium deposit. Athabasca Basin, Saskatchewan. GAC-MAC 2011 Conference, Ottawa, May 25–27, 2011 (abstract online at http://gac.esd.mun.ca/gac_2011/search_abs/sub_program.asp?sess=98&form=10&abs_no=462).
Richard, A., Pettke, T., Cathelineau, M., Boiron, M.C., Mercadier, J., Cuney, M., Derome, D., 2010. Brine-rock interaction in the Athabasca basement (McArthur River U deposit, Canada): consequences for fluid chemistry and uranium uptake. Terra Nova 22, 303–308.
Rieder, M., Cavazzini, G., D'Yakonov, Y.S., Frank-Kamanetskii, V.A., Gottardi, G., Guggenheim, S., Koval', P.V., Müller, G., Neiva, A.M.R., Radoslovich, E.W., Robert, J.L., Sassi, F.P., Takeda, H., Weiss, Z., Wones, D.R., 1998. Nomenclature of the micas. The Canadian Mineralogist 36, 41–48.
Rosenberg, P.E., 2002. The nature, formation, and stability of end-member illite: a hypothesis. American Mineralogist 87, 103–107.
Rozenson, I., Heller-Kallai, L., 1978. Reduction and oxidation of Fe^{3+} in dioctahedral smectites—III.*oxidation of octahedral iron in montmorillonite. Clays and Clay Minerals 26, 88–92.
Sattonnay, G., Ardois, C., Corbel, C., Lucchini, J.F., Barthe, M.-F., Garrido, F., Gosset, D., 2001. Alpha-radiolysis effects on UO_2 alteration in water. Journal of Nuclear Materials 288, 11–19.
Stumm, W., Morgan, J.J., 1996. Aquatic Chemistry: Chemical Equilibria and Rates in Natural Waters, third ed. Wiley-Interscience, New York.
Wallis, R.H., Saracoglu, N., Brummer, J.J., Golightly, J.P., 1985. The geology of the McClean uranium deposits, northern Saskatchewan. In: Sibbald, T.I.I., Petruk, W. (Eds.), Geology of Uranium Deposits, Canadian Institute of Mining, Metallurgy and Petroleum, Special Volume 32, pp. 101–131.
Walshe, J.L., 1986. A six-component chlorite solid-solution model and the conditions of chlorite formation in hydrothermal and geothermal systems. Economic Geology 81, 681–703.
Wasyliuk, K.R., 2001. Petrogenesis of the kaolinite-group minerals in the eastern Athabasca Basin of northern Saskatchewan: applications to uranium mineralization. Unpublished M.Sc. thesis, Saskatoon, Canada, University of Saskatchewan (140 pp.).
Weaver, C.E., Wampler, J.M., Pecuil, T.E., 1967. Mössbauer analysis of iron in clay minerals. Science 156, 504–508.
Wenner, D.B., Taylor Jr., H.P., 1971. Temperatures of serpentinization of ultramafic rocks based on O^{18}/O^{16} fractionation based on coexisting serpentine and magnetite. Contributions to Mineralogy and Petrology 32, 165–185.
Wilson, M.R., Kyser, T.K., 1987. Stable isotope geochemistry of alteration associated with the Key Lake uranium deposit, Canada. Economic Geology 82, 1540–1557.
Wilson, M.R., Kyser, T.K., Mehnart, H.H., Hoeve, J., 1987. Changes in the H–O–Ar isotope composition of clays during retrograde alteration. Geochimica et Cosmochimica Acta 51, 869–878.
Yeh, H.W., 1980. D/H ratios and late-stage dehydration of shales during burial. Geochimica et Cosmochimica Acta 44, 341–352.
Zang, W., Fyfe, W.S., 1995. Chloritization of the hydrothermally altered bedrock at the Igarapé Bahia gold deposit, Carajás, Brazil. Mineralium Deposita 30, 30–38.
Zazzi, A., Hirsch, T.K., Leonova, E., Kaikkonen, A., Grins, J., Annersten, H., Edén, M., 2006. Structural investigations of natural and synthetic chlorite minerals by X-ray diffraction, Mössbauer spectroscopy, and solid-state nuclear magnetic resonance. Clays and Clay Minerals 54, 252–265.
Zhang, G., Wasyliuk, K., Pan, Y., 2001. The characterization and quantitative analysis of clay minerals in the Athabasca Basin, Saskatchewan: application of short-wave infrared reflectance spectroscopy. The Canadian Mineralogist 39, 1347–1363.